Nonthermal Effects on X-ray Radiative Signatures of High-Energy-Density Plasmas Produced in Laboratory Z-pinches

Ryan R. Childers

Safronova HED Plasma Research Group
University of Nevada, Reno – Physics Department

SSGF/LRGF Program Review 2023
San Francisco, CA - June 29, 2023

Outline

I. Plasma Overview: Pulsed-power Z-pinch Plasmas

II. Influence of X-pinch Load Geometry on Bright Spot Production & K-shell Radiation

III. Monte Carlo Radiation Transport of Nonthermal x-ray Fe fluorescence in a MagLIF plasma

IV. Conclusions/Acknowledgements

Plasmas span a range of temperature and densities

- High-energy, ionized state of matter
  - extreme pressures, temperatures, densities

- Locally-generated EM fields,
- Global-collective particle behavior,
- Hydrodynamic properties
- Highly Radiative

- Conditions categorize type of plasma
  - "Cold", nonthermal
  - "Warm", dense
  - "Hot", thermal

Can mix in HED plasmas

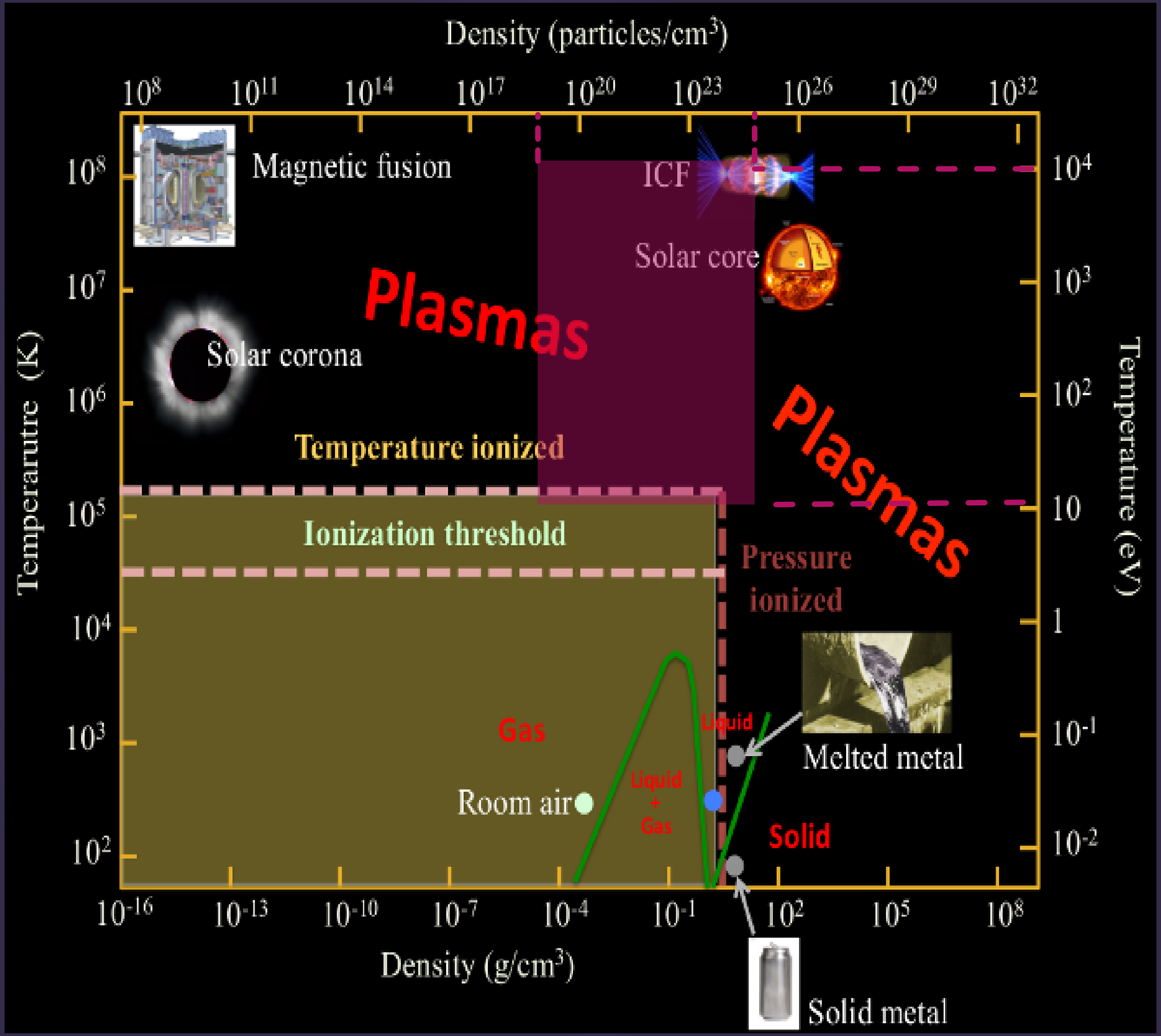

Image Credit: Los Alamos National Laboratory (https://www.lanl.gov/projects/dense-plasma-theory/background/physical-regimes.php)

Plasma processes come in two primary flavors

- Thermal ("hot" line emission)
  - Multiply ionized (high internal energy) ions
  - Maxwellian (isotropic) particle energy distribution
  - Ions & electrons = same temperature
  - Thermal radiation ("ionic")
- Nonthermal ("cold" line emission)
  - Weakly ionized (low internal energy) ions
  - Non-Maxwellian particle distribution
  - Different ion & electron temperatures
  - Nonthermal radiation ("characteristic")

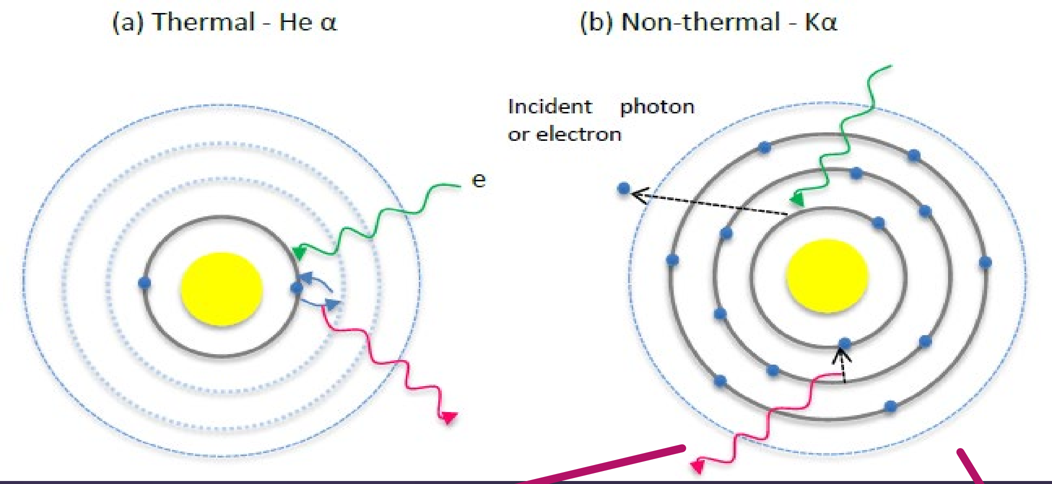

Illustration of the kinetics of (a) thermal Heα emission and (b) non-thermal Kα emission[1]

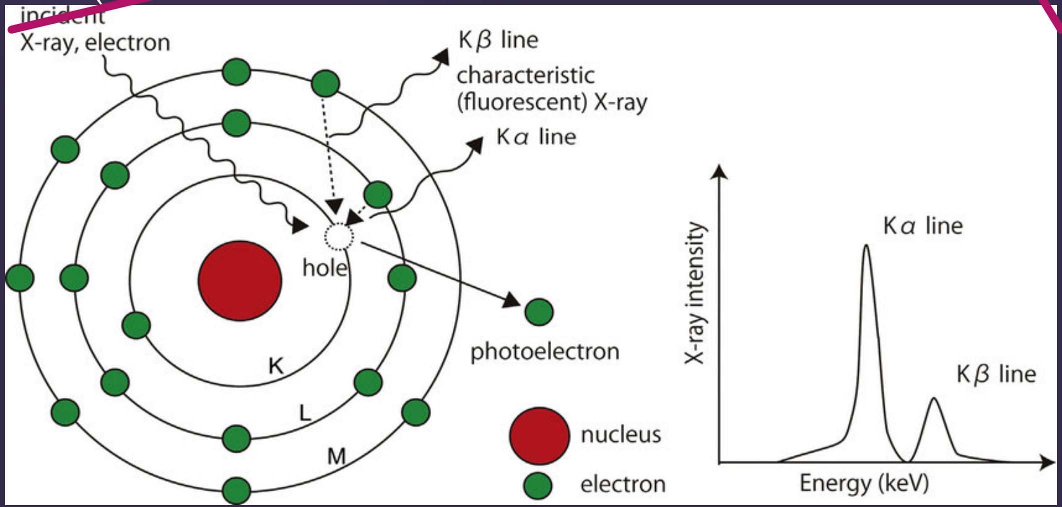

Illustration of nonthermal K-shell relaxation process & spectral line profile[2]

[1]D. J. Ampleford et al., Sandia report SAND2015-10453 (2015)

[2]M. Uo et al. Jap. Den. Sci. Rev. (2014)

Nonthermal radiation valuable for assessing conditions of cooler regions of capsule implosions

- Nonthermal x-ray spectroscopy is significant for stockpile stewardship missions related to ICF, HED x-ray studies, etc.
- Nonthermal x-rays can provide insight to capsule preheat from nonthermal electrons
- Mid-Z impurities in various capsule design can provide diagnostic fiducials for constraining temperature, density, etc.

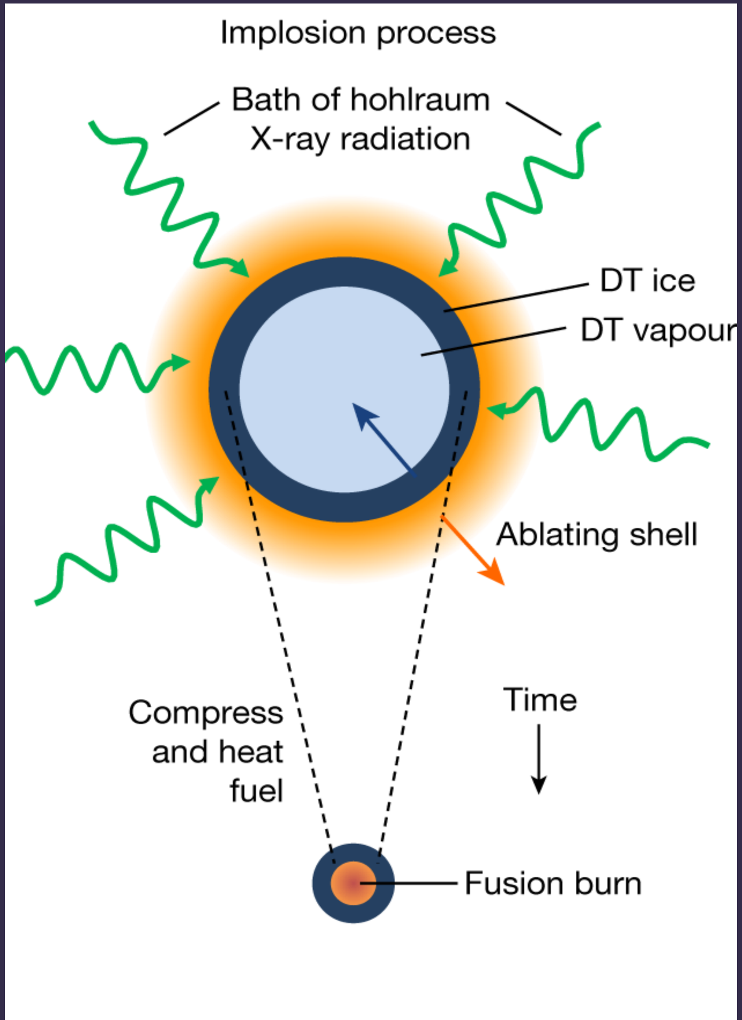

Image: Zylstra, A.B., Hurricane, O.A., Callahan, D.A. et al. Burning plasma achieved in inertial fusion. Nature 601, 542–548 (2022). https://doi.org/10.1038/s41586-021-04281-w

Nonthermal radiation valuable for assessing conditions of cooler regions of capsule implosions

- Nonthermal x-ray spectroscopy is significant for stockpile stewardship missions related to ICF, HED x-ray studies, etc.
- Nonth
capsul
- Mid-Z impurities in various capsule design can provide diagnostic fiducials for constraining temperature, density, etc.

<u>Goal:</u> Perform a comprehensive investigation on the influence of nonthermal effects on x-ray radiation in laboratory plasmas, with an emphasis on production efficiency and origin.

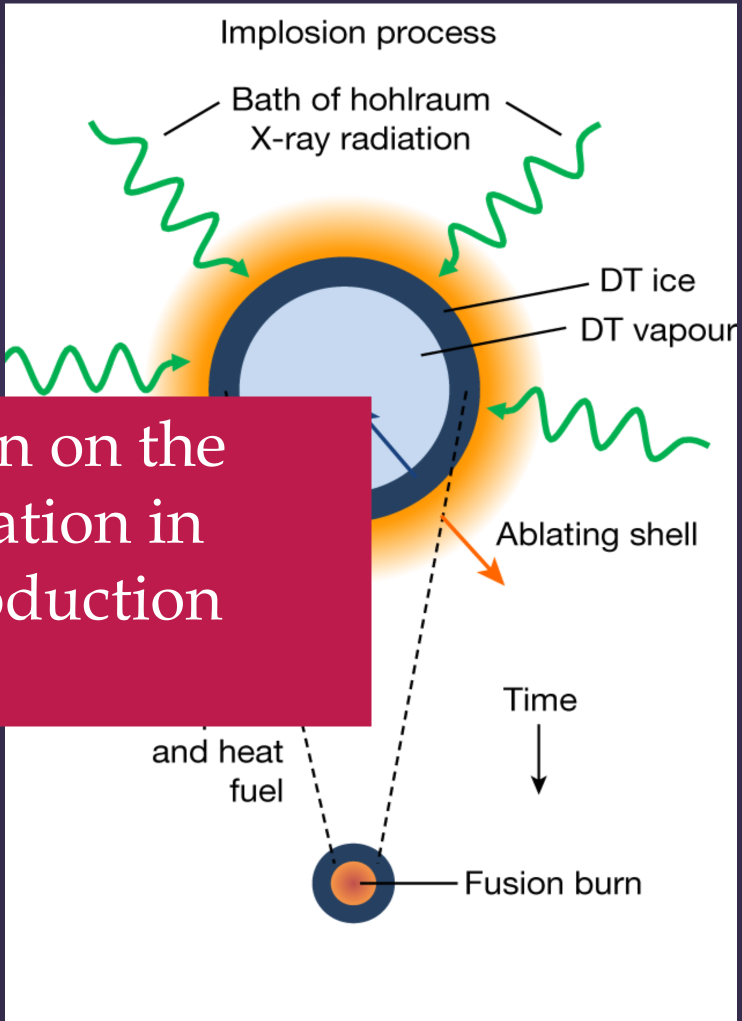

Z-pinches produce magnetically-confined HED plasma sources with high x-ray yield

Plasma is created by sublimating solid material through rapid heating (ohmic or laser).

1. Electric potential created across electrode gap
2. Current is pulsed through pathway medium
   - Wires, Foil, Gas, etc
3. Azimuthal magnetic field created about current carrying wires, confining material
4. $\vec{J} \times \vec{B}$ Lorentz force acts radially to pinch material towards pinch axis

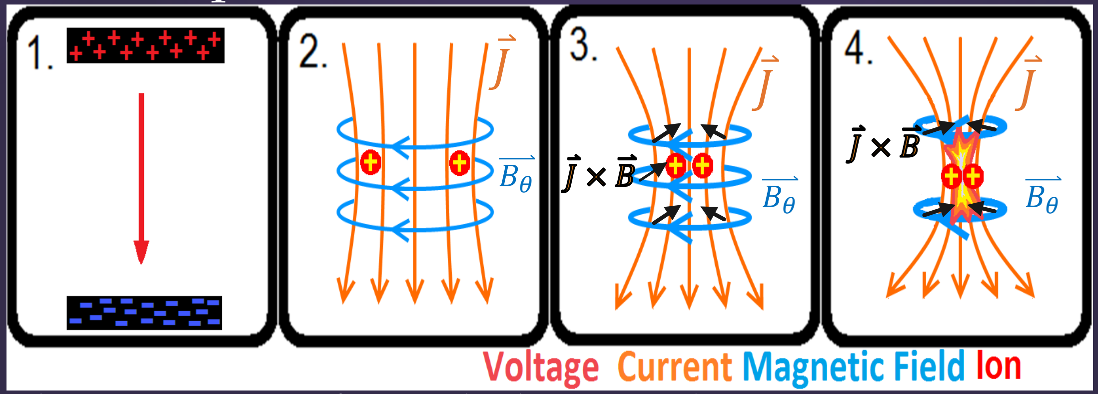

Schematic cartoon of Z-pinch plasma production process

Pre pulsed wire x-pinch[3]

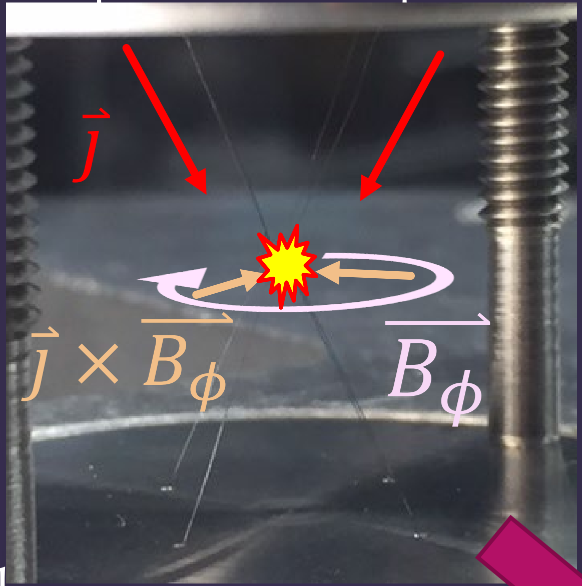

Fuel-filled cylindrical liner[1]

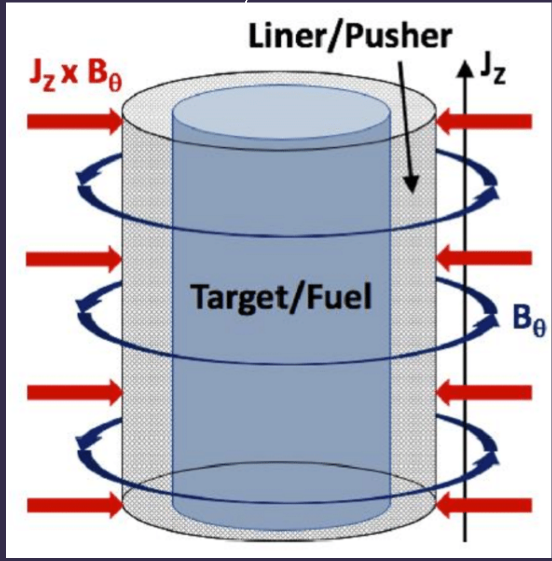

Bright spot clusters (x-ray image)

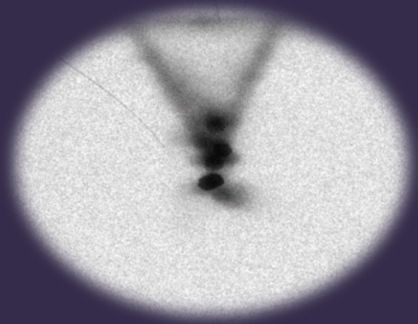

Z-pinches produce magnetically-confined HED plasma sources with high x-ray yield

Plasma is created by sublimating solid material through rapid heating (ohmic or laser).

1. Electric potential created across electrode gap
2. Current is pulsed through pathway medium
   - Wires, Foil, Gas, etc
3. Azimuthal magnetic field created about current carrying wires, confining material
4. $\vec{J} \times \vec{B}$ Lorentz force acts radially to pinch material towards pinch axis

Pre pulsed wire x-pinch[3]

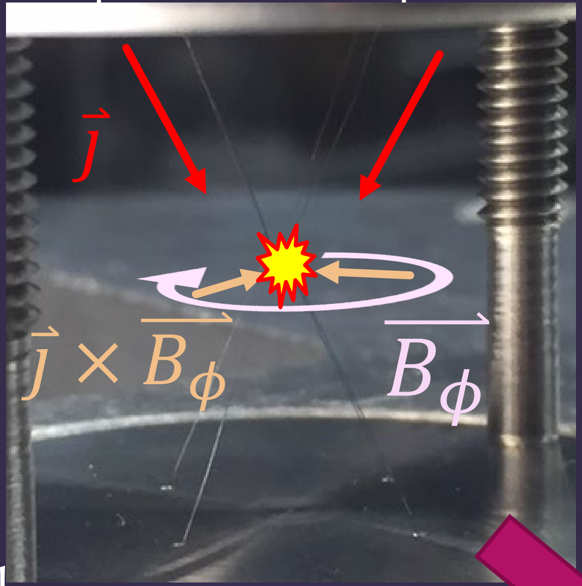

Fuel-filled cylindrical liner[1]

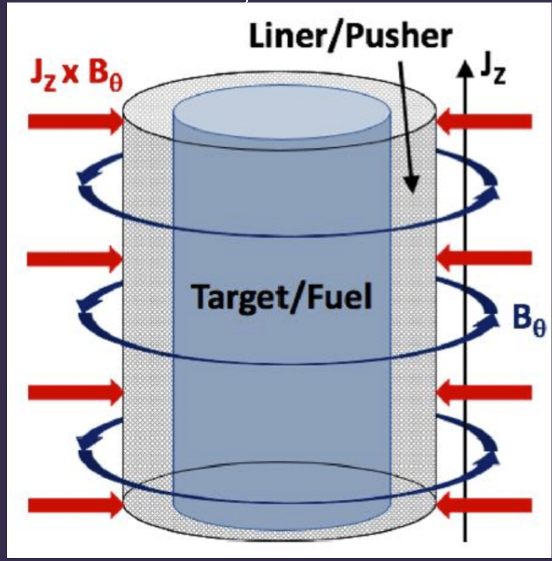

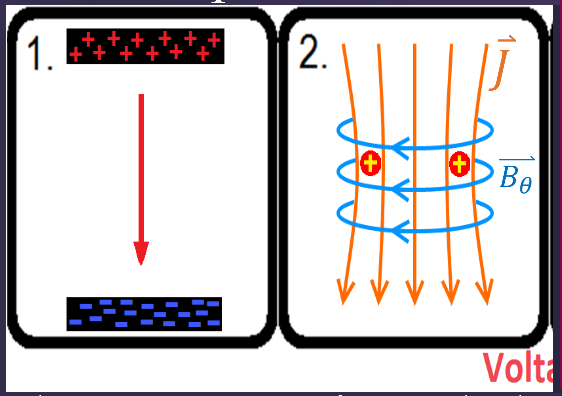

Schematic cartoon of Z-pinch plasma production process

Bright spot production

- Dense ($\gtrsim 10^{18}$ cm^{-3})
- High temperature ($\gtrsim$ 1 keV) plasma
- Bursts of x-ray emission (x-ray bursts)
- Production of hot, nonthermal electrons

Bright spot clusters (x-ray image)

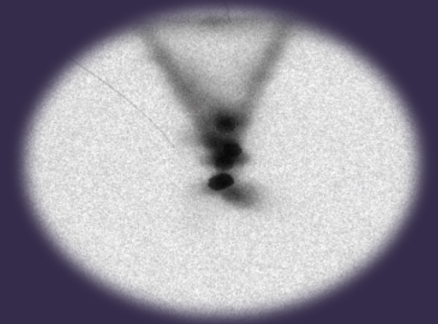

[1]E. Ruskov *et al.*, Physics of Plasmas **27**, 042709 (2020) [2]V. L. Kantsyrev *et al.*, *Phys. of Plasma*, **15**, 030704 (2008) [3]R. R. Childers et al., IEEE Trans Plasma Sci. 46: 3820 (2018)

Outline

I. Plasma Overview: Pulsed-power Z-pinch Plasmas

II. Influence of X-pinch Load Geometry on Bright Spot Production & K-shell Radiation

III. Monte Carlo Radiation Transport of Nonthermal x-ray Fe fluorescence in a MagLIF plasma

IV. Conclusion/Acknowledgements

X-pinch experiments are performed on the pulsed-power 1 MA Zebra Generator at UNR

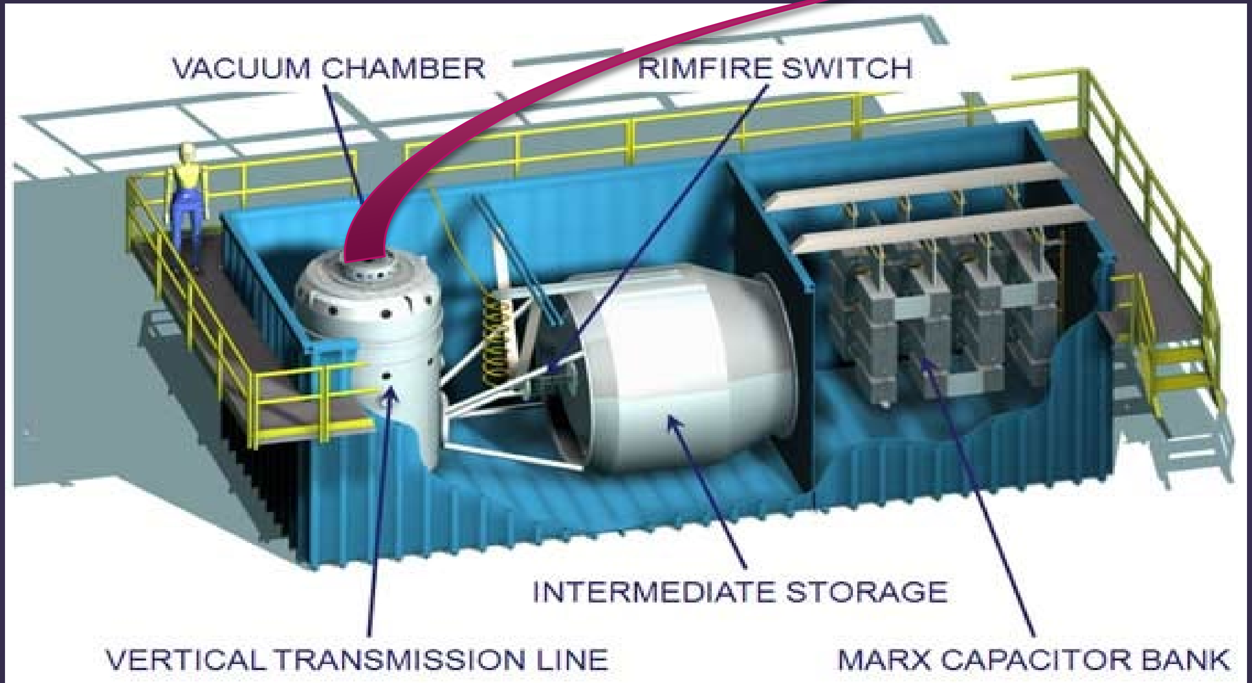

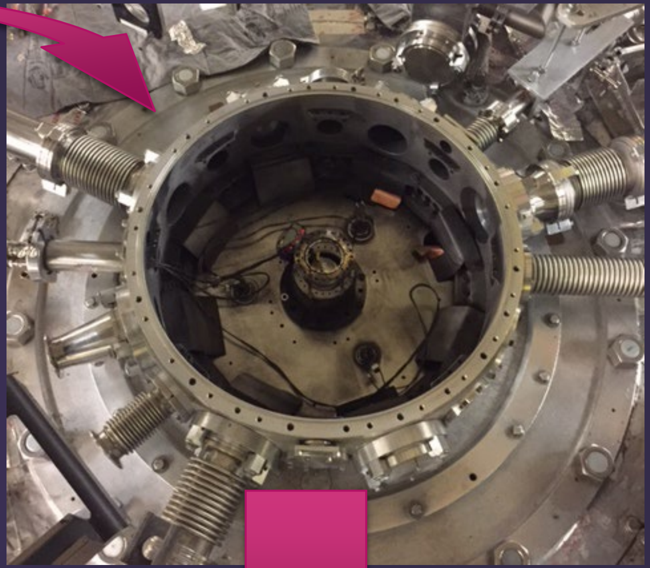

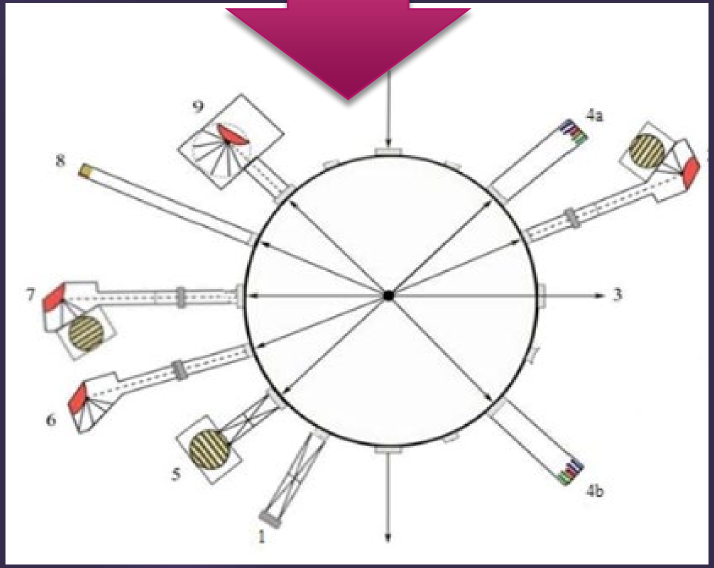

- 2 TW pulsed power generator (~1 MA current)
  - Current rise time: 100 ns
  - Total energy: 150 kJ
  - Housed at University of Nevada, Reno (UNR)[1,2]

[1]B. S. Bauer et al., *12th IEEE Int. Pulsed Power Conf. Dig. Tech. Papers* **2**, 1045 (1999) [2]V. L. Kantsyrev *et al.*, *Phys. Plasmas*, **10**, 2519-2526 (2003)

X-pinch wire load geometry varied to study influence on K-shell radiation and bright spot production[1]

- Stainless steel (69% Fe, 20% Cr, 9% Ni) wire loads
  - 31° or 62.5° interwire angle
  - 4 wires, 40 μm diameter, 830 μg total mass
- Bright spots (> 3 keV) measured to determine size and quantity
- Diagnostic signals analyzed to characterize x-ray emission properties of bright spot sources
- Time-integrated x-ray Fe-Cr-Ni spectra are analyzed using non-LTE CRM.

X-pinch load in Zebra[2]

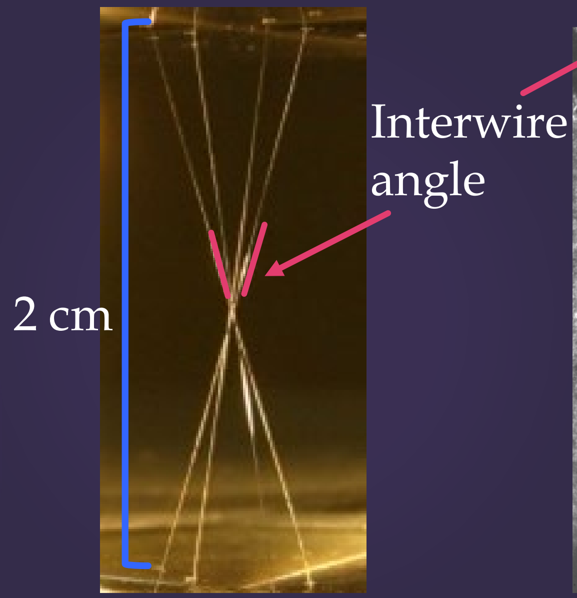

Shadowgrams of X-pinch wire loads

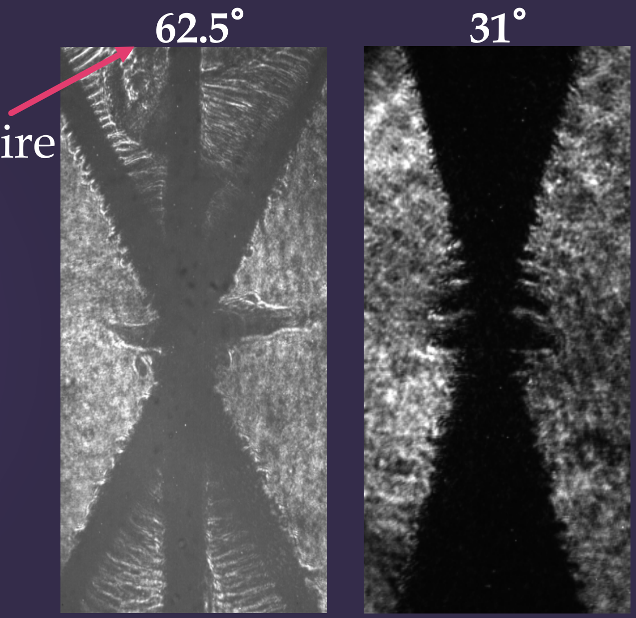

Zebra Shot #	Interwire Angle	Current [MA]	Rad Yield [kJ]
1588	31°	0.91	16.7
1589	62.5°	0.94	14.6
1590	31°	0.92	17.1
1591	31°	0.92	15.5
1592	62.5°	0.93	11.3

[1]R.R. Childers *et al.*, *JQSRT*, **303**, 108586 (2023) [2]V. L. Kantsyrev *et al.*, *Phys. Plasmas*, **10**, 2519-2526 (2003)

X-pinch wire load geometry varied to study influence on K-shell radiation and bright spot production[1]

- Stainless steel (69% Fe, 20% Cr, 9% Ni) wire loads
  - 31° or 62.5° interwire angle
  - 4 wires, 40 μm diameter, 830 μg total mass

X-pinch load in Zebra[2]

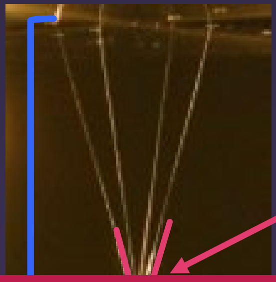

Shadowgrams of X-pinch wire loads

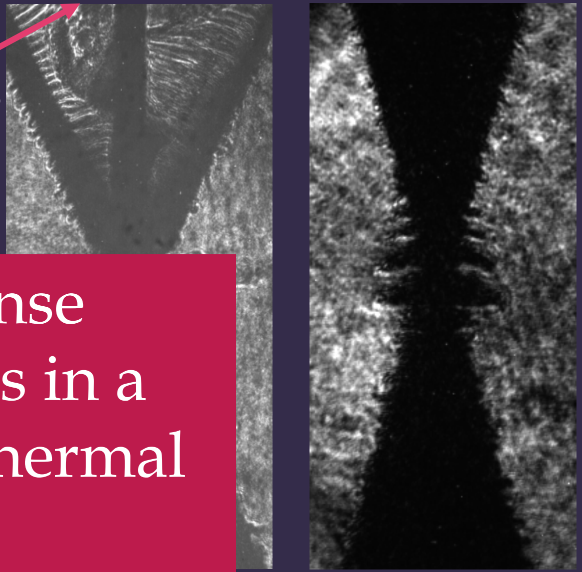

- Bright spots (> 3
  size and quantity

Goal: Investigate how to efficiently generate intense thermal and nonthermal x-ray radiative signatures in a single X-pinch plasma, with an emphasis on nonthermal electron production.

- Diagnostic signals analyzed to characterize x-ray emission properties of bright spot sources

- Time-integrated x-ray Fe-Cr-Ni spectra are analyzed using non-LTE CRM.

Zebra Shot #	Interwire Angle	Current [MA]	Rad Yield [kJ]
1588	31°	0.91	16.7
1589	62.5°	0.94	14.6
1590	31°	0.92	17.1
1591	31°	0.92	15.5
1592	62.5°	0.93	11.3

[1]R.R. Childers *et al.*, *JQSRT*, **303**, 108586 (2023) [2]V. L. Kantsyrev *et al.*, *Phys. Plasmas*, **10**, 2519-2526 (2003)

FWHM analysis performed on x-ray emitting source size

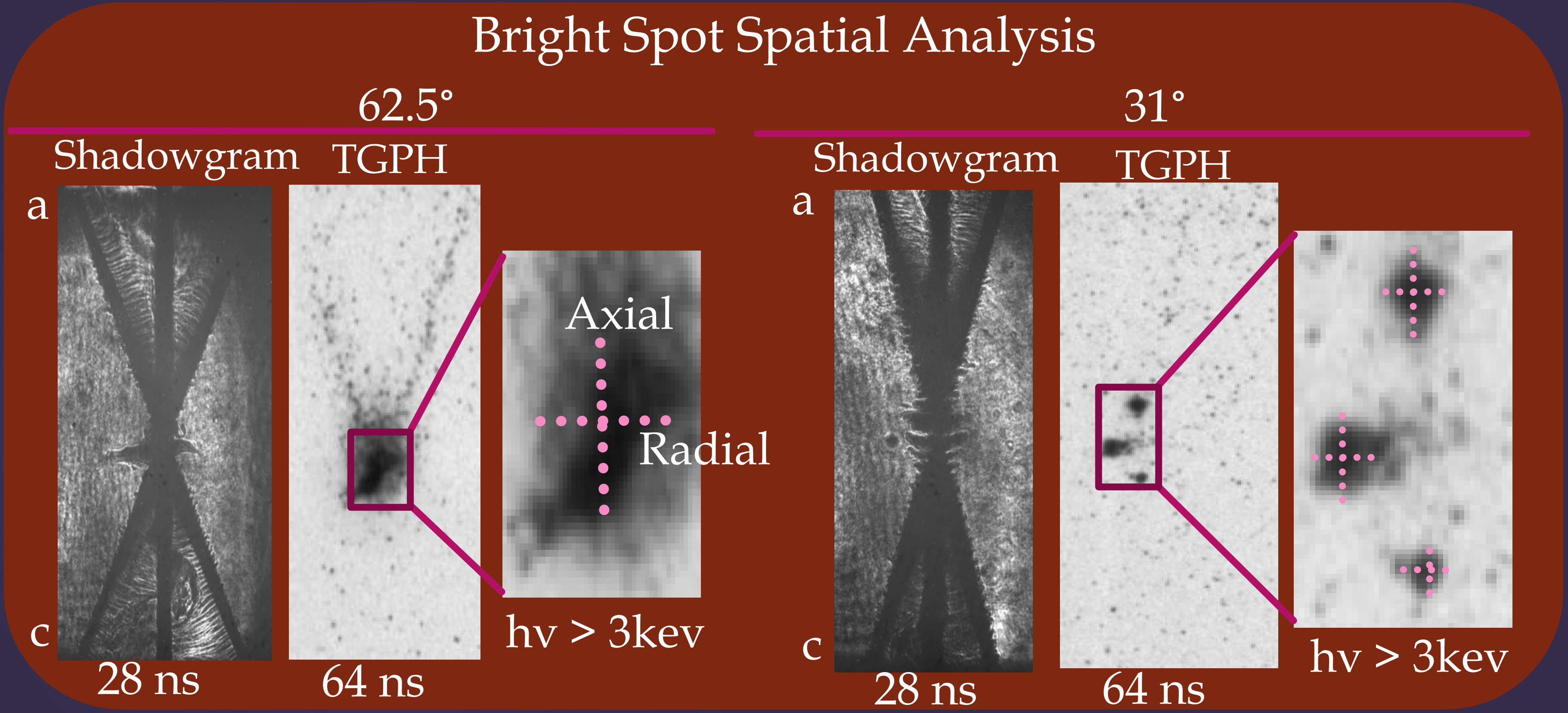

R.R. Childers et al., JQSRT, 303, 108586 (2023)

FWHM analysis performed on x-ray emitting source size

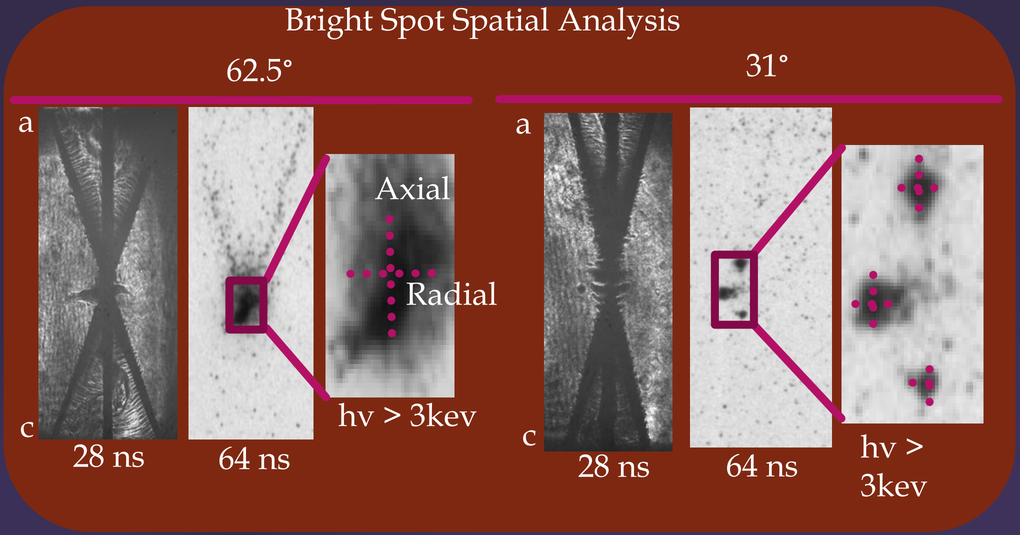

62.5°

- Single, larger bright spots at cross point (≥ 1.0 mm²)

31°

- Multiple smaller bright spots along pinch axis (≤ 0.5 mm²)

Time-averaged spatial measurement results

Geometry	Zebra Shot	Bright Spots	FWHM		
			Axial ± σ_A [μm]	Radial ± σ_R [μm]	Area ± σ_{Ar} [mm²]
Small-angle	1588	2	535 ± 216	417 ± 137	0.25 ± 0.13
	1590	3	519 ± 324	663 ± 443	0.46 ± 0.43
	1591	3	561 ± 245	578 ± 151	0.35 ± 0.18
Large-angle	1589	1	937 ± 187	1280 ± 314	1.16 ± 0.37
	1592	1	920 ± 498	1080 ± 313	0.98 ± 0.60

FWHM analysis performed on time-resolved x-ray diode signals

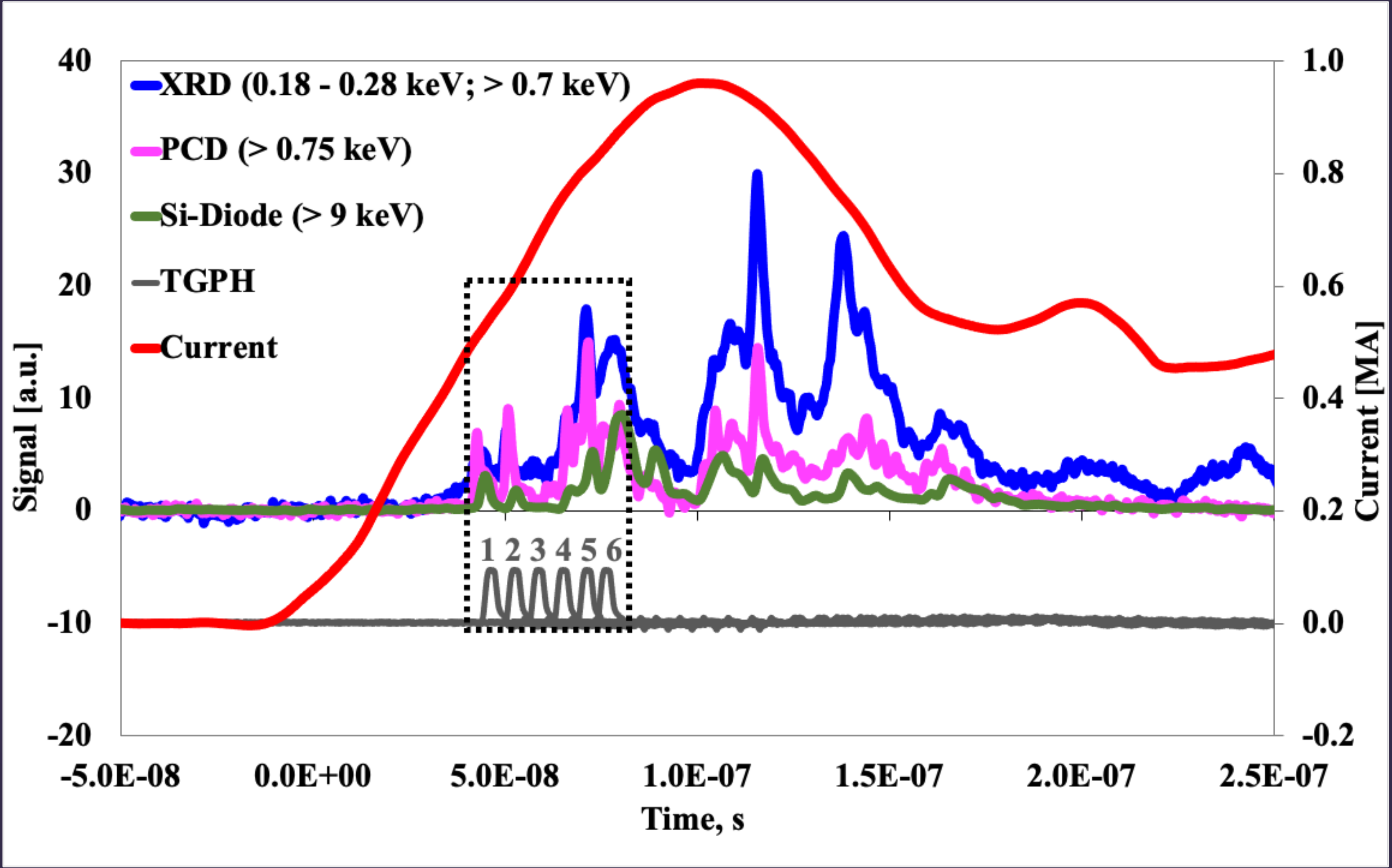

FWHM analysis performed on time-resolved x-ray diode signals

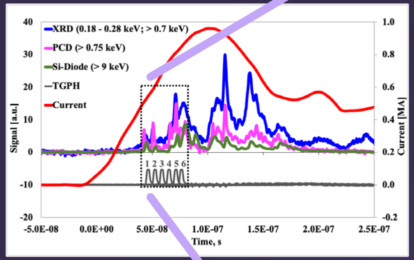

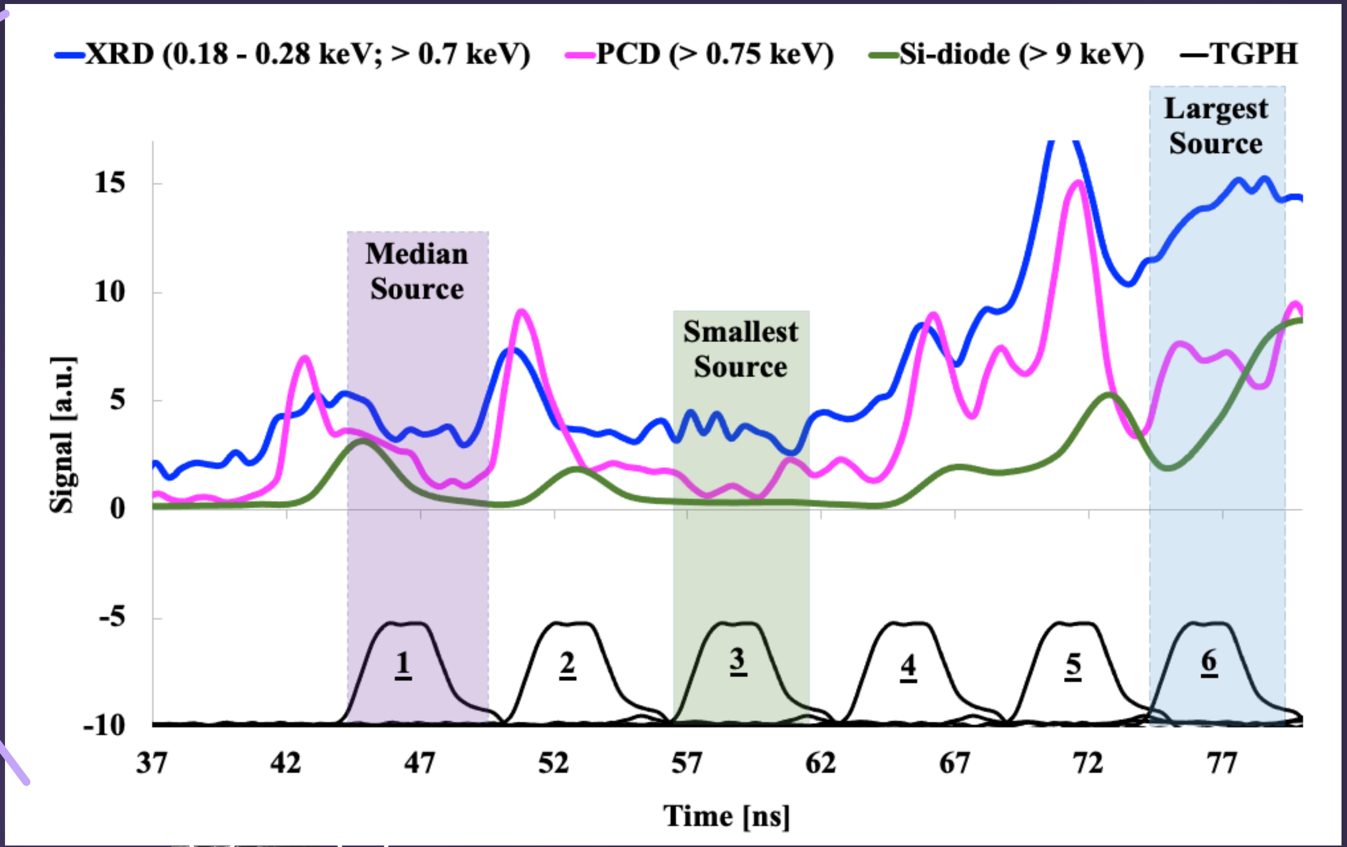

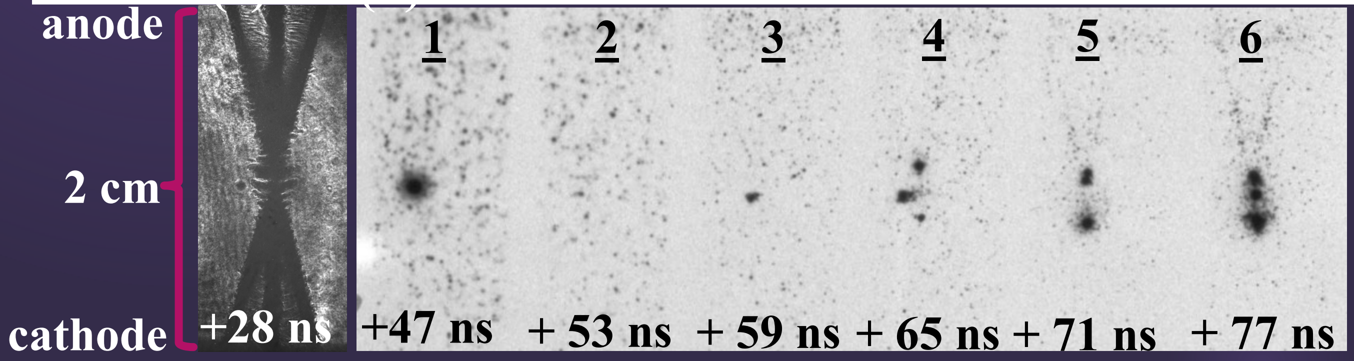

FWHM analysis performed on time-resolved x-ray diode signals

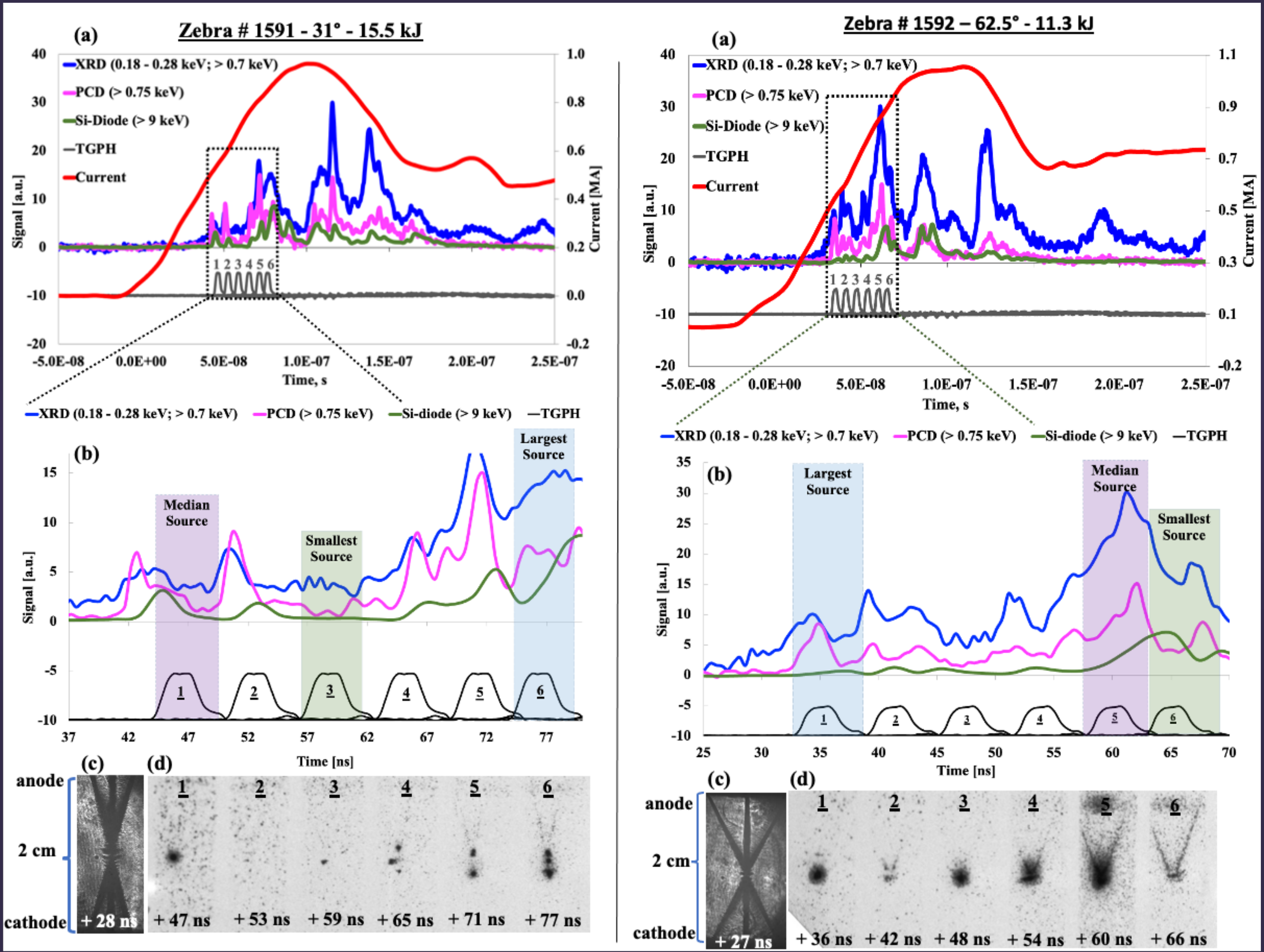

62.5°

- Dynamic soft x-ray (> 3 keV keV) signal
- Radiation yields ≤ 14.6 kJ
- Source size varies proportionally with current

31°

- Notable hard x-ray (> 9 keV) signal dynamics
- Radiation yields ≥ 15.5 kJ
- Source size decreases with increasing current (more pinching)

R.R. Childers et al., JQSRT, 303, 108586 (2023)

Synthetic modeling reveals distinct x-ray radiative properties for each X-pinch geometry

- Nonthermal "cold" plasma region:
  - $T_e \leq 50$ eV, $n_e \sim 10^{18}$ cm^{-3}
  - Fe, Cr, & Ni ions of Ne-like & lower

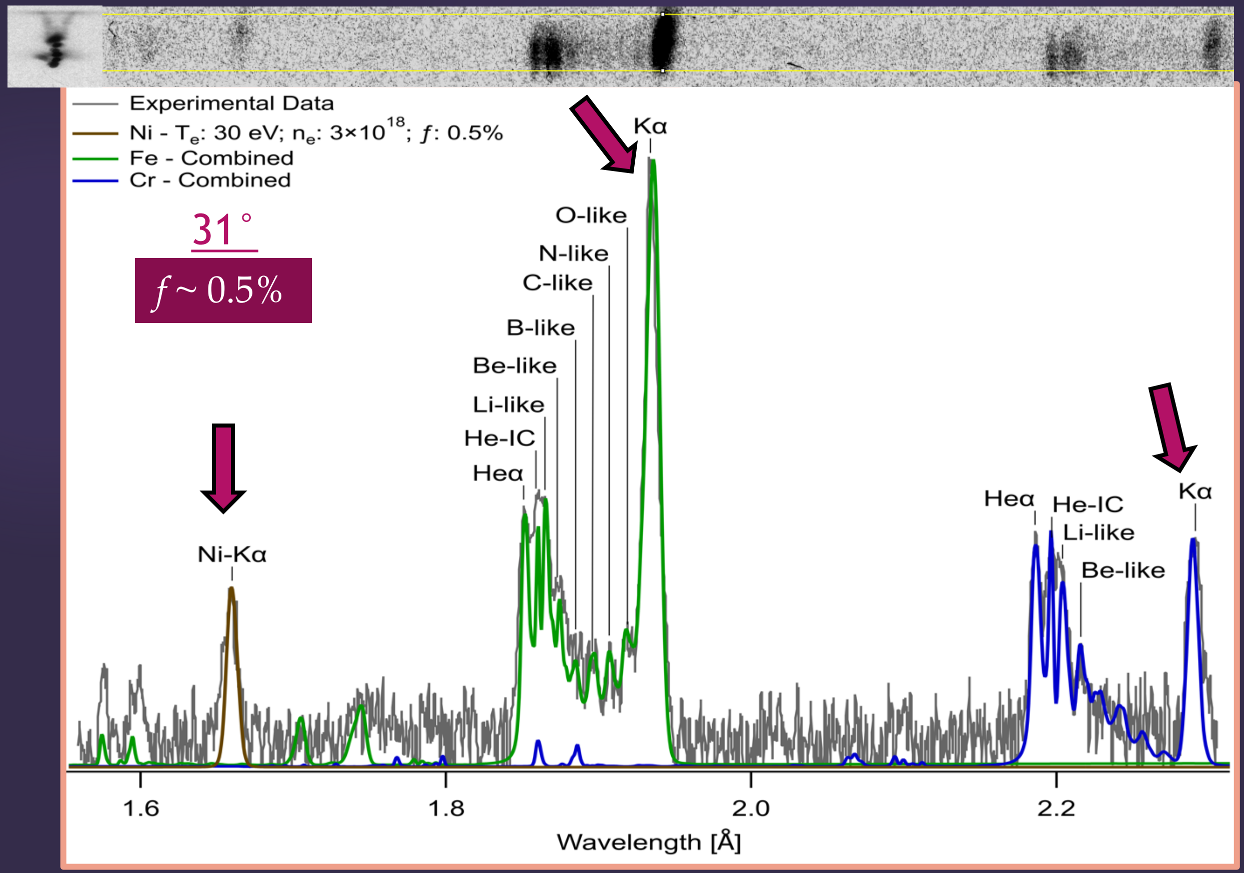

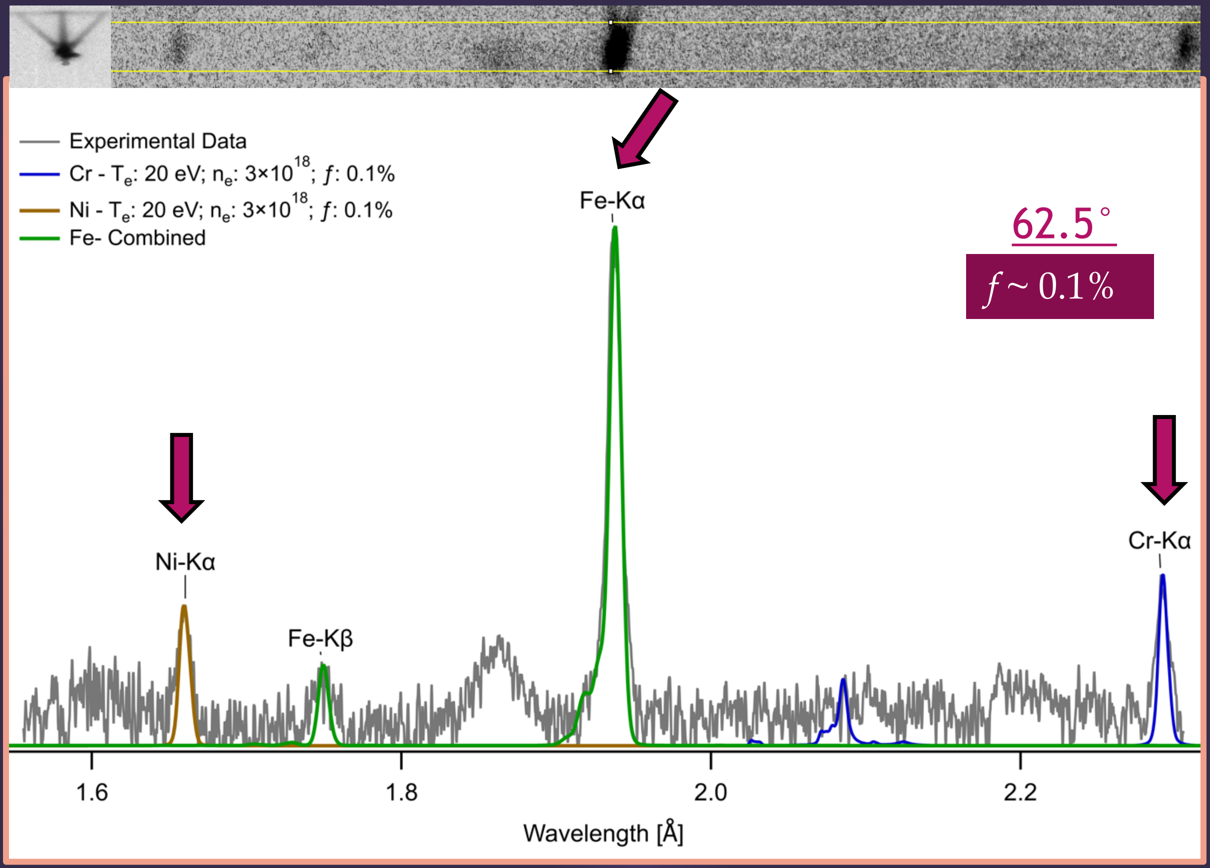

Synthetic modeling reveals distinct x-ray radiative properties for each X-pinch geometry

- Nonthermal "cold" plasma region:
  - $T_e \leq 50$ eV, $n_e \sim 10^{18}$ cm^{-3}
  - Fe, Cr, & Ni ions of Ne-like & lower
- Intermediate "Satellite" region:
  - $T_e \leq 1000$ eV, $n_e \sim 10^{19}$ cm^{-3}
  - Fe O-like to Li-like Kα satellites

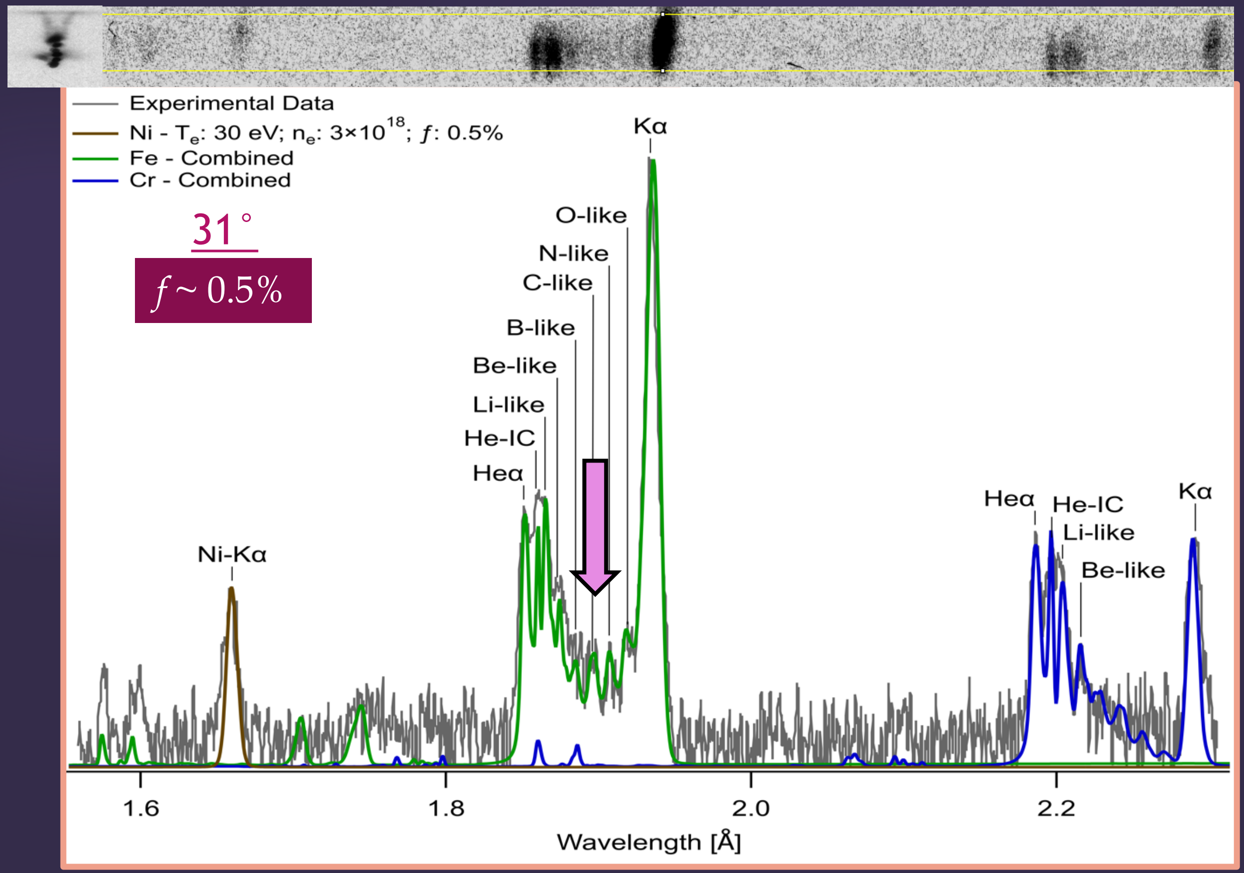

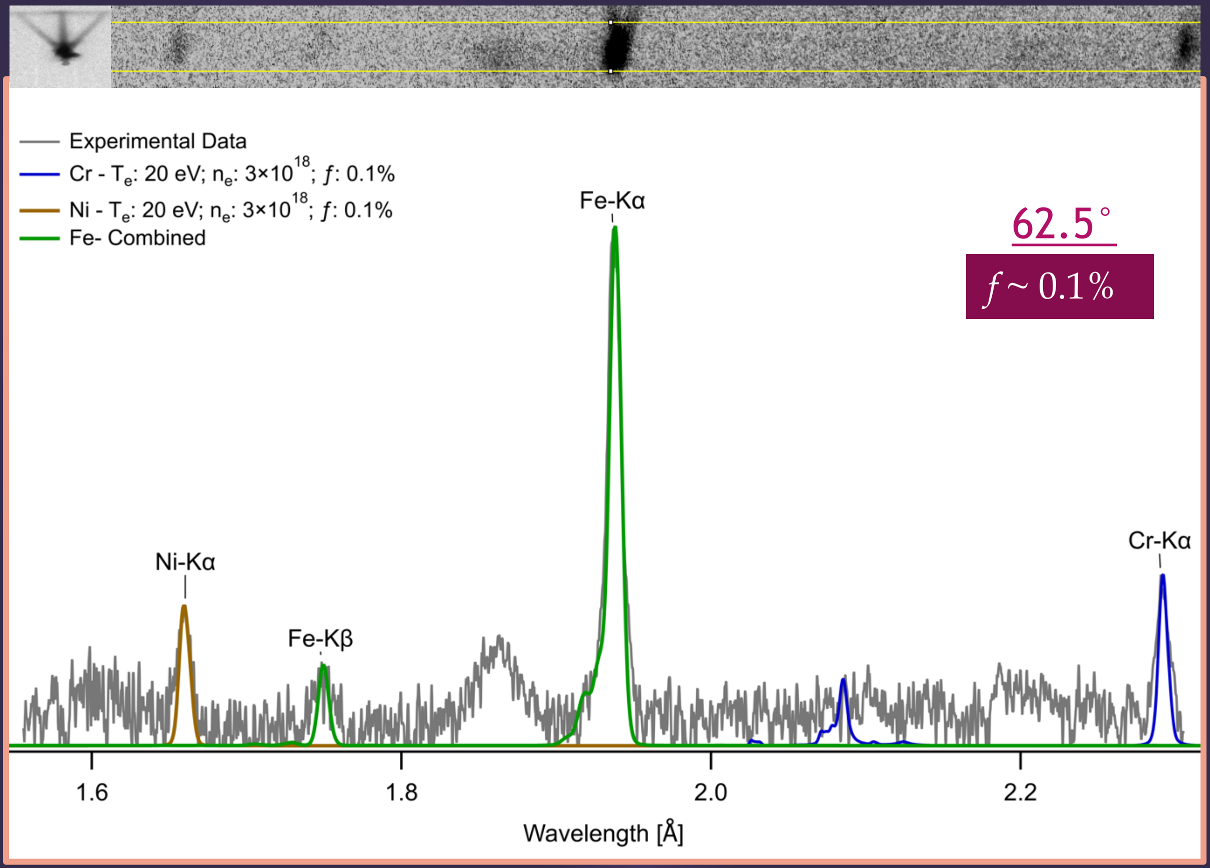

Synthetic modeling reveals distinct x-ray radiative properties for each X-pinch geometry

- Nonthermal "cold" plasma region:
  - $T_e \leq 50$ eV, $n_e \sim 10^{18}$ cm^{-3}
  - Fe, Cr, & Ni ions of Ne-like & lower

- Intermediate "Satellite" region:
  - $T_e \leq 1000$ eV, $n_e \sim 10^{19}$ cm^{-3}
  - Fe O-like to Li-like Kα satellites

- Thermal "hot" plasma region:
  - $T_e \leq 2.0$ keV, $n_e \sim 10^{20}$ cm^{-3}
  - Fe & Cr He-like and Li-like ions

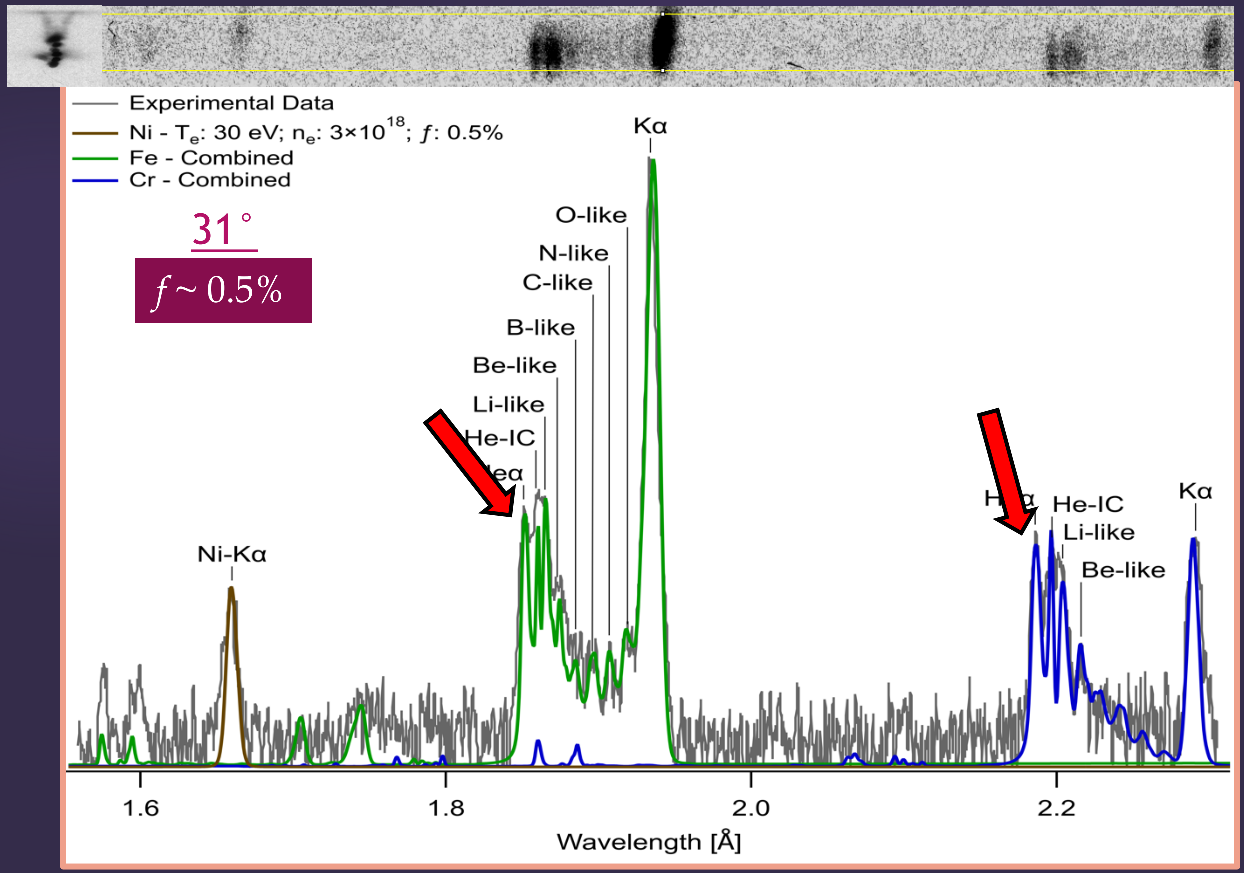

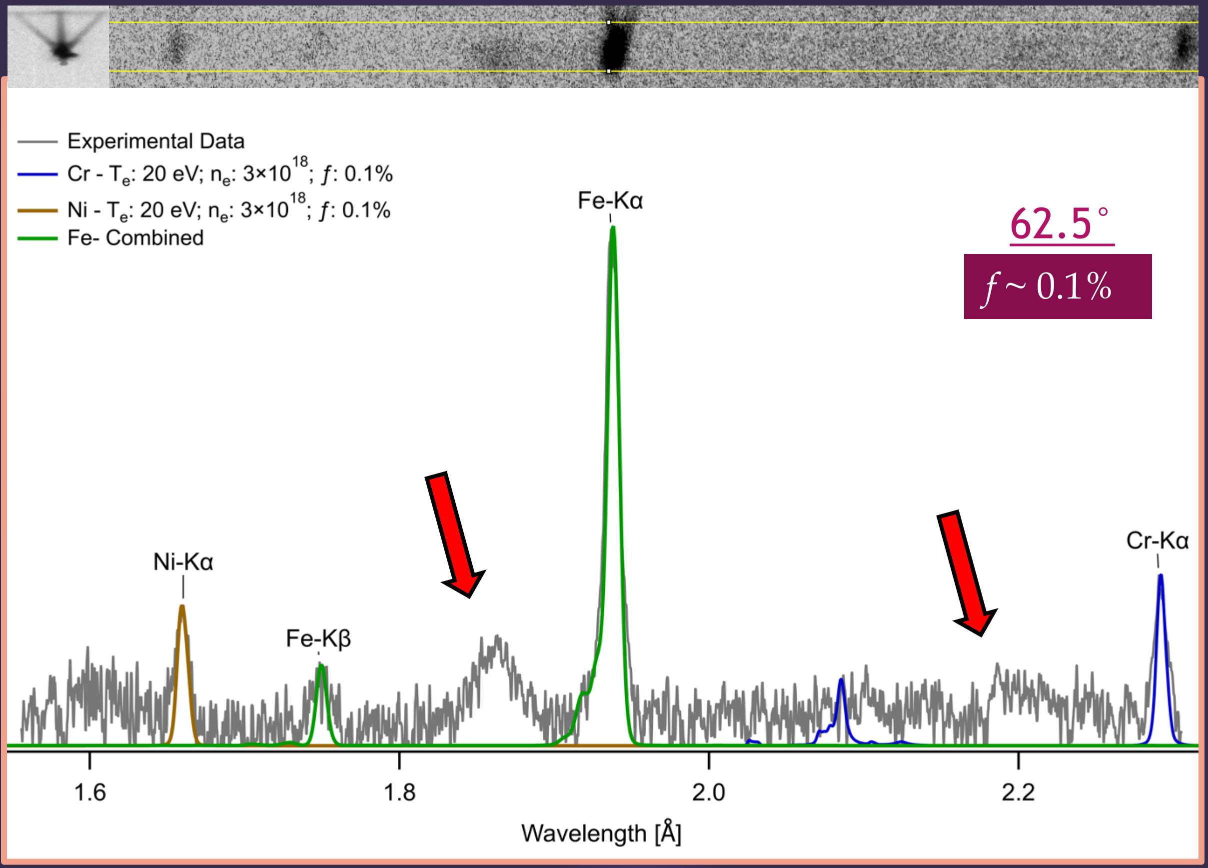

R.R. Childers et al., JQSRT, 303, 108586 (2023)

Synthetic modeling reveals distinct x-ray radiative properties for each X-pinch geometry

- Nonthermal "cold" plasma region:
  - $T_e \leq 50$ eV, $n_e \sim 10^{18}$ cm^{-3}
  - Fe, Cr, & Ni ions of Ne-like & lower
- Intermediate "Satellite" region:
  - $T_e \leq 1000$ eV, $n_e \sim 10^{19}$ cm^{-3}
  - Fe O-like to Li-like Kα satellites
- Thermal "hot" plasma region:
  - $T_e \leq 2.0$ keV, $n_e \sim 10^{20}$ cm^{-3}
  - Fe & Cr He-like and Li-like ions

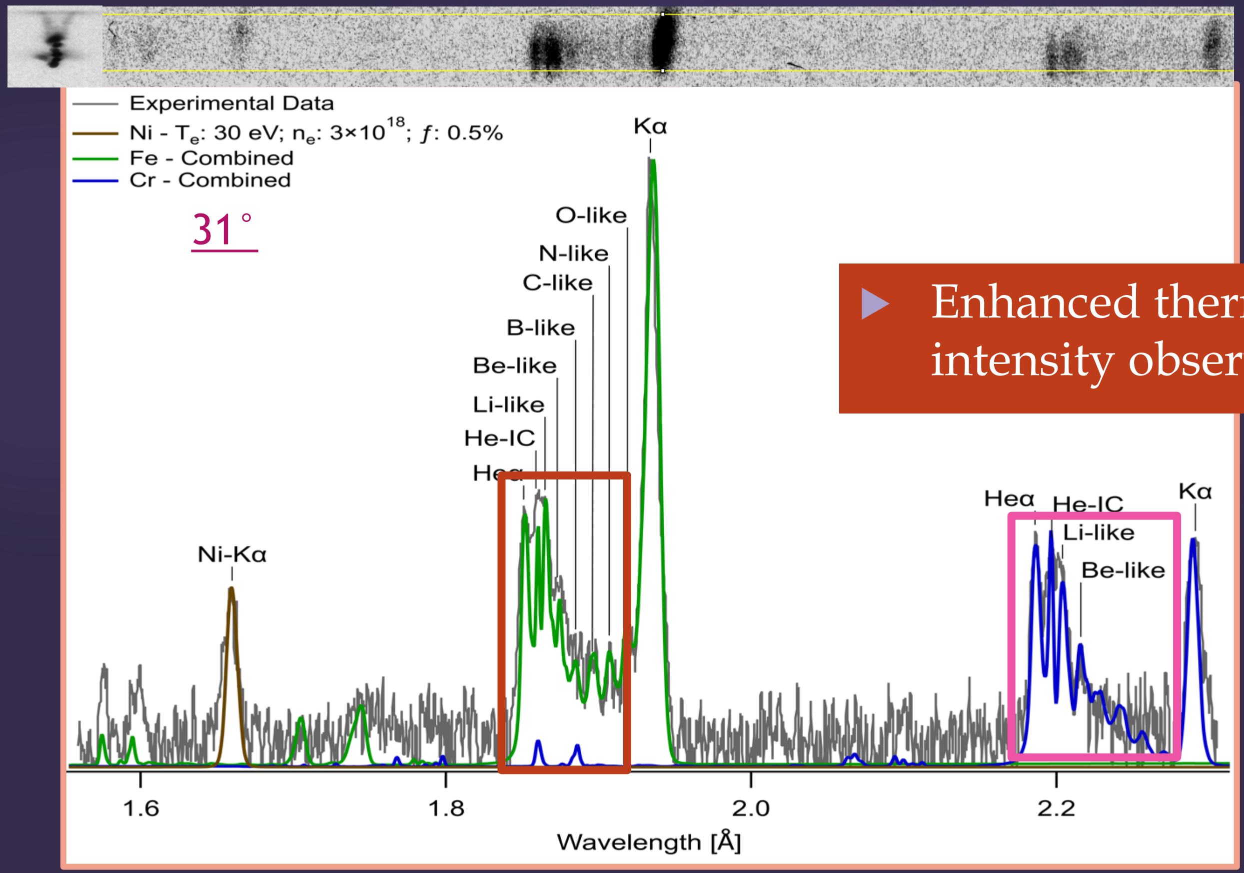

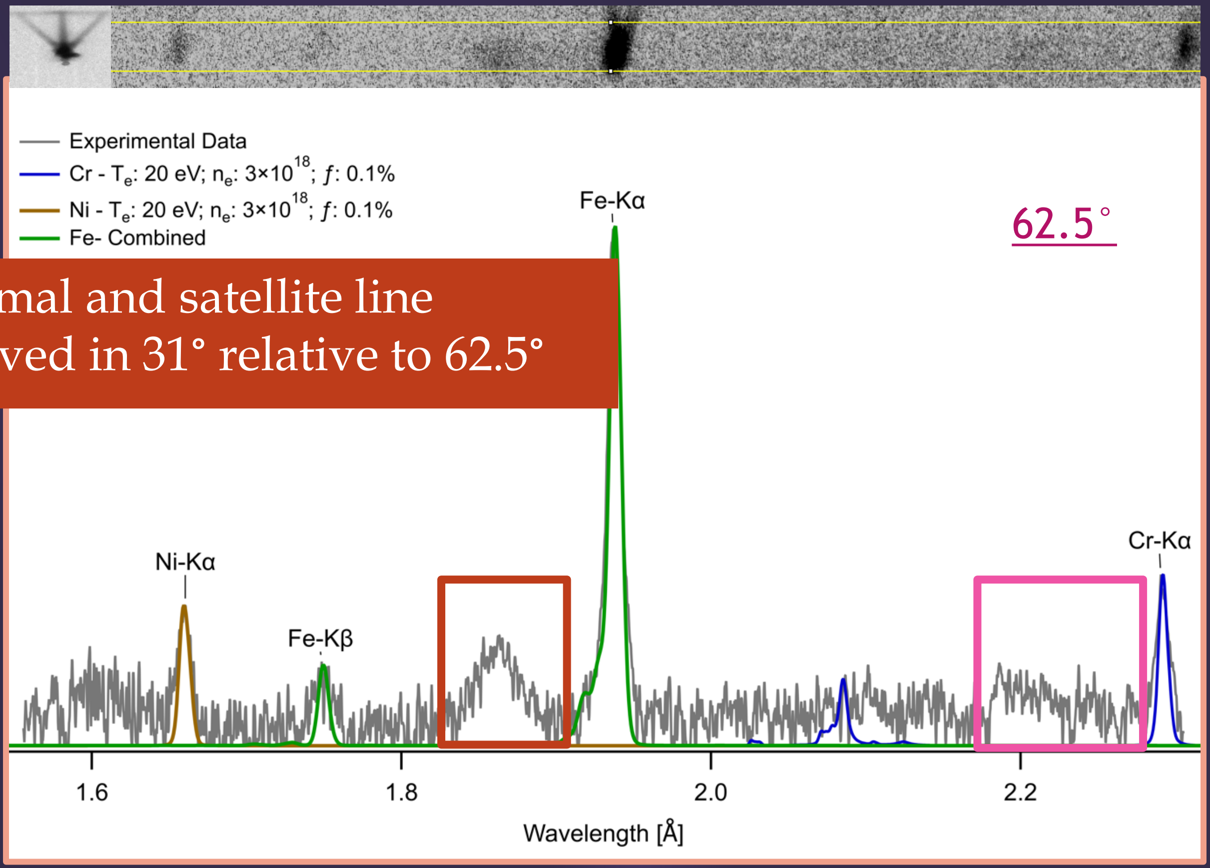

- Enhanced thermal and satellite line intensity observed in 31° relative to 62.5°

R.R. Childers et al., JQSRT, 303, 108586 (2023)

Synthetic modeling reveals distinct x-ray radiative properties for each X-pinch geometry

- Nonthermal "cold" plasma region:
  - $T_e \leq 50$ eV
  - Fe, Cr, & N

- Intermediate "Satellite" region:

- Thermal "hot" plasma region:
  - $^{-3}$
  - ions

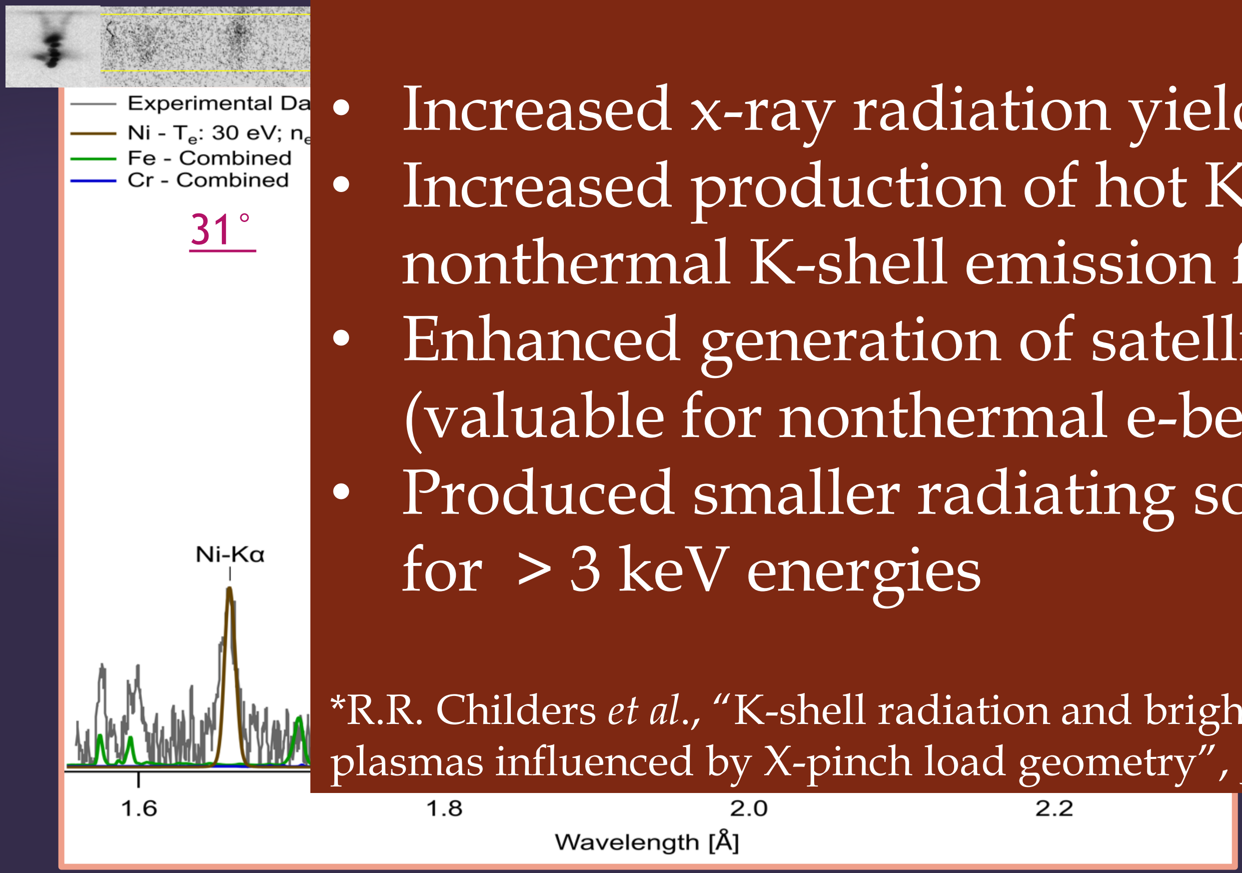

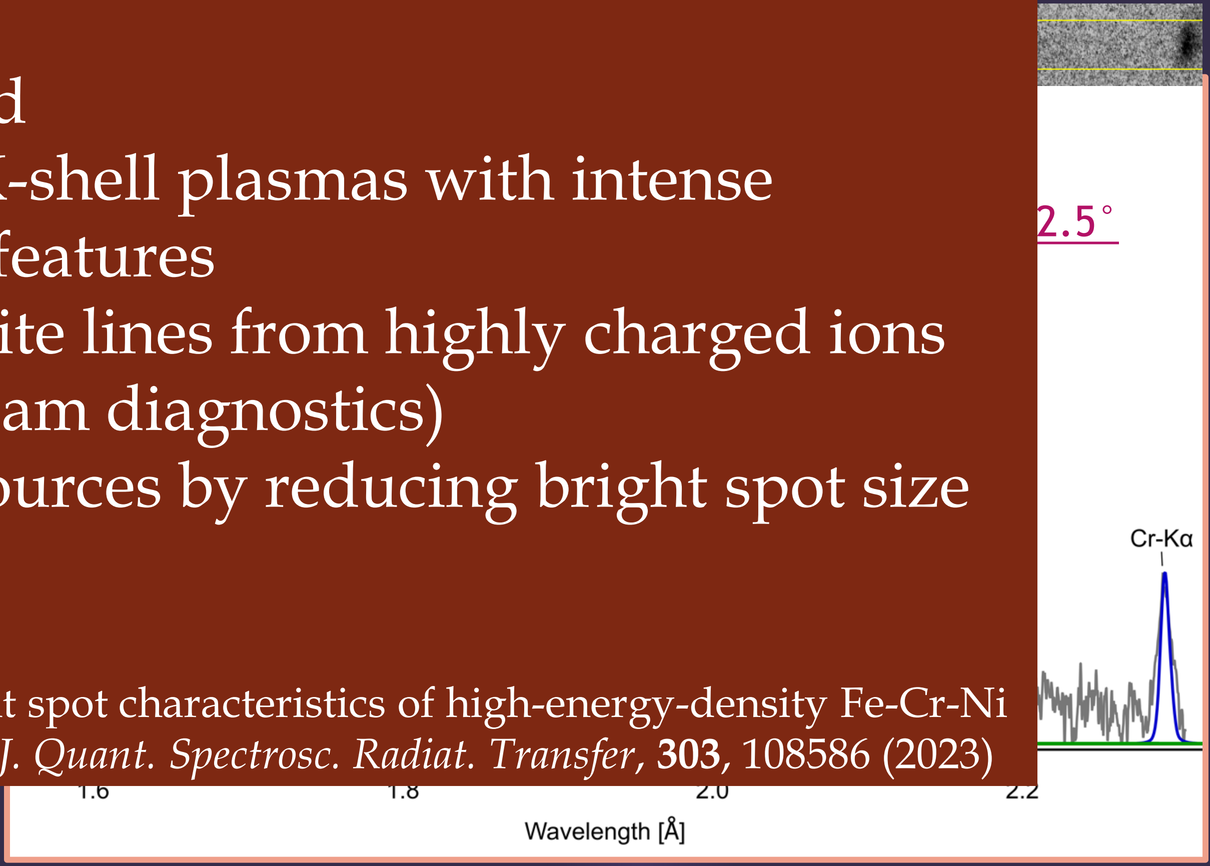

Results*

By decreasing the interwire angle, we have successfully:

- Increased x-ray radiation yield
- Increased production of hot K-shell plasmas with intense nonthermal K-shell emission features
- Enhanced generation of satellite lines from highly charged ions (valuable for nonthermal e-beam diagnostics)
- Produced smaller radiating sources by reducing bright spot size for > 3 keV energies

*R.R. Childers *et al.*, "K-shell radiation and bright spot characteristics of high-energy-density Fe-Cr-Ni plasmas influenced by X-pinch load geometry", *J. Quant. Spectrosc. Radiat. Transfer*, **303**, 108586 (2023)

Outline

I. Plasma Overview: Pulsed-power Z-pinch Plasmas

II. Influence of X-pinch Load Geometry on Bright Spot Production & K-shell Radiation

III. Monte Carlo Radiation Transport of Nonthermal x-ray Fe fluorescence in a MagLIF plasma

IV. Conclusion/Acknowledgements

Radiation transport is investigated in a dense MagLIF plasma using a novel Monte Carlo post-processor

- X-ray fluorescence studied in MagLIF plasmas on Z.
- MagLIF[1] produced by
  - 2.5 kJ laser preheat of fusion core
  - Implosion by current-driven axial magnetic flux
  - Z-pinch compression to inertially confine fusion core
- Two new computational packages developed:
  - A screened-hydrogenic atomic data package
  - A novel Monte Carlo Radiation Transport code
- Monte Carlo Rad transport utility = spatial analysis of nonthermal particle origin

MagLIF Scheme[2]

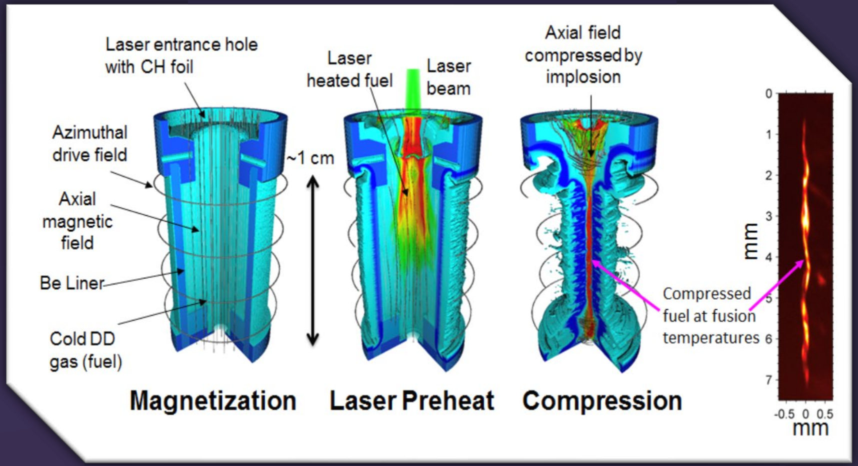

Fluorescence process[3]

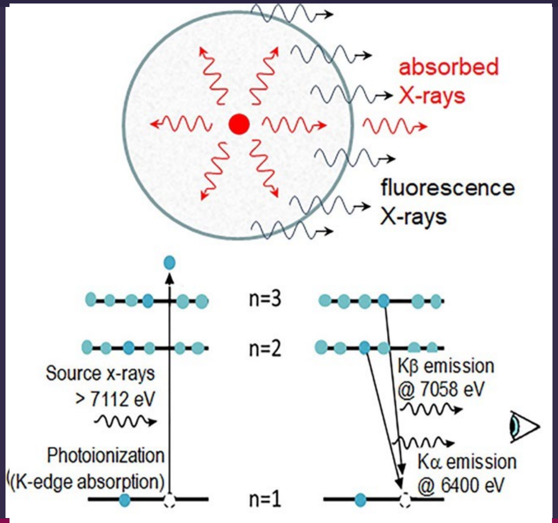

[1]M. R. Gomez et al., Phys. Plasmas, 22, 056306 (2015) [2]K.D. Hahn et al., J. Phys: Conf. Series 717:012020 (2016) [3]S. B. Hansen *et al.*, *Phys. Plasmas*, **25**, 056301 (2018)

Radiation transport is investigated in a dense MagLIF plasma using a novel Monte Carlo post-processor

- X-ray fluorescence studied in MagLIF plasmas on Z.
- MagLIF[1] p…
  - …
- …ore
- …d:
- Mo… …nalysis of nonthermal particle origin

MagLIF Scheme[2]

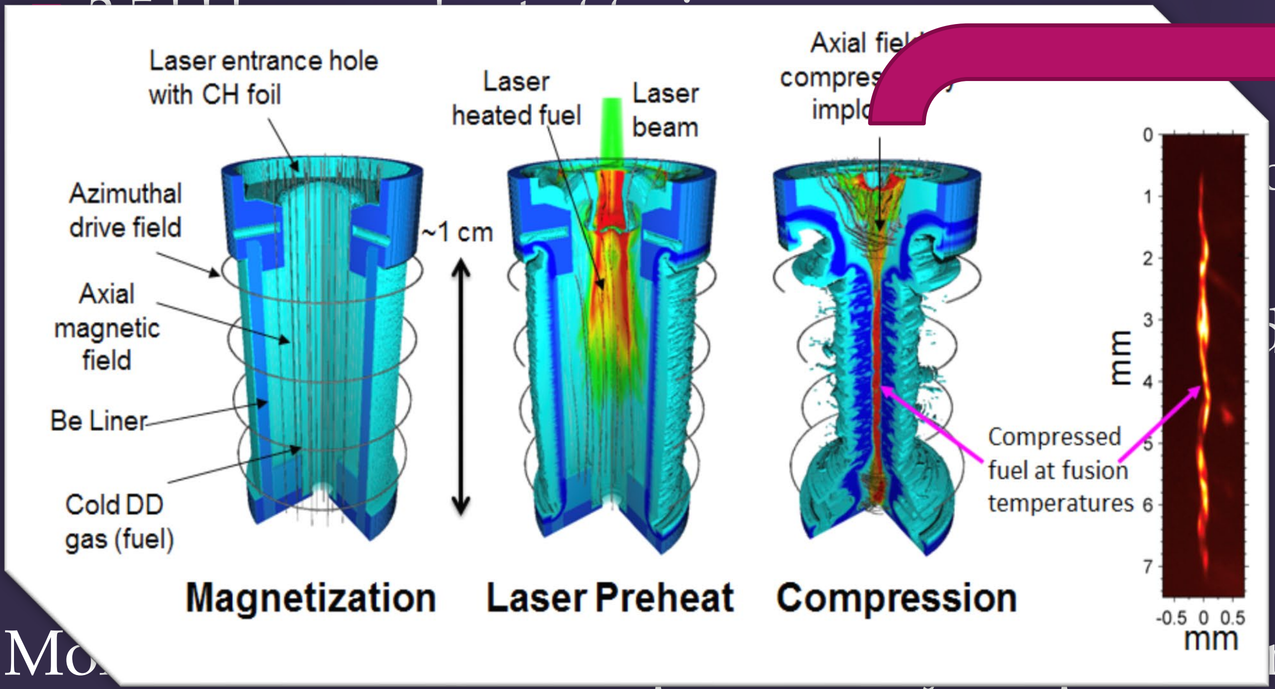

Fluorescence process[3]

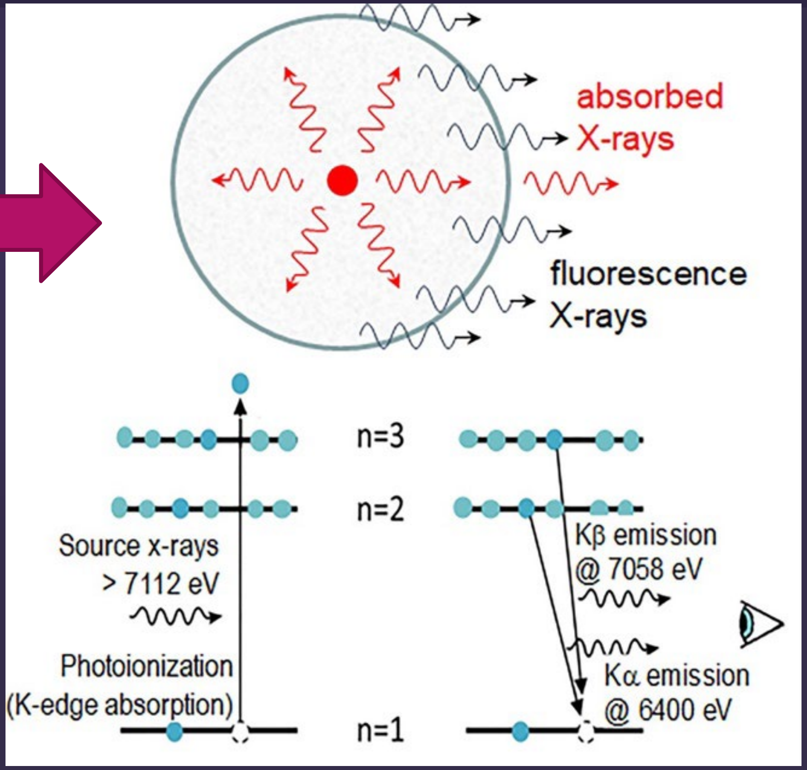

Radiation transport is investigated in a dense MagLIF plasma using a novel Monte Carlo post-processor

- X-ray fluorescence studied in MagLIF plasmas on Z.
- MagLIF[1] produced by
  - 2.5 kJ laser preheat of fusion core
  - Imp
  - Z-p

Goal: Explore spatial origins of nonthermal fluorescence production in a dense MagLIF liner plasma shell.

- Two new computational packages developed:
  - A screened-hydrogenic atomic data package
  - A novel Monte Carlo Radiation Transport code
- Monte Carlo Rad transport utility = spatial analysis of nonthermal particle origin

MagLIF Scheme[2]

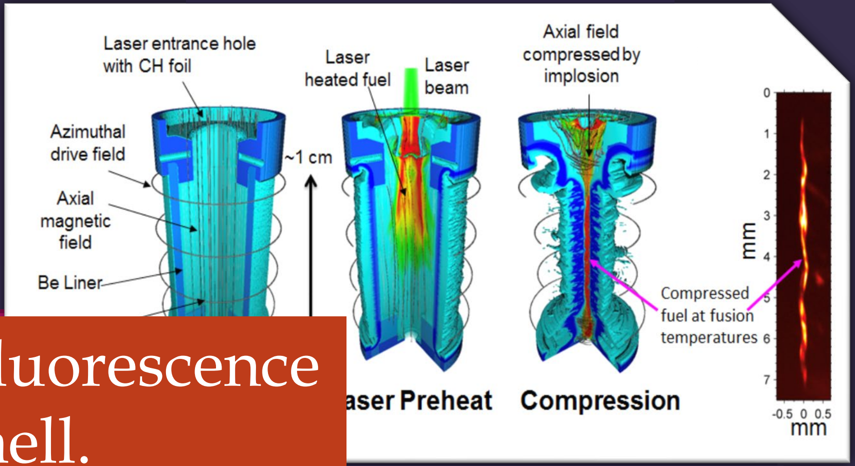

Fluorescence process[3]

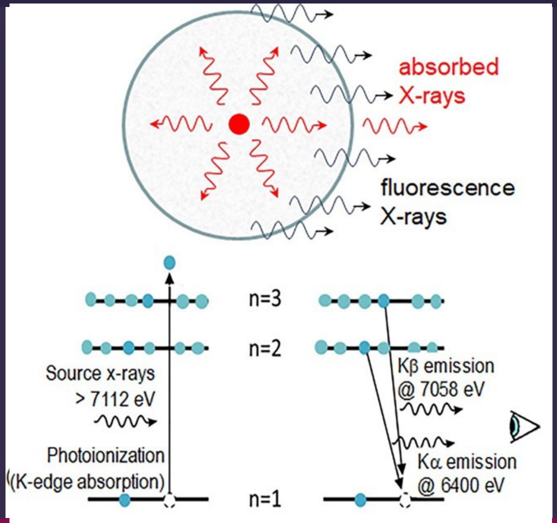

A newly constructed computational package uses Monte Carlo and screened-hydrogenic-atom schemes to post-process radiation transport in MagLIF

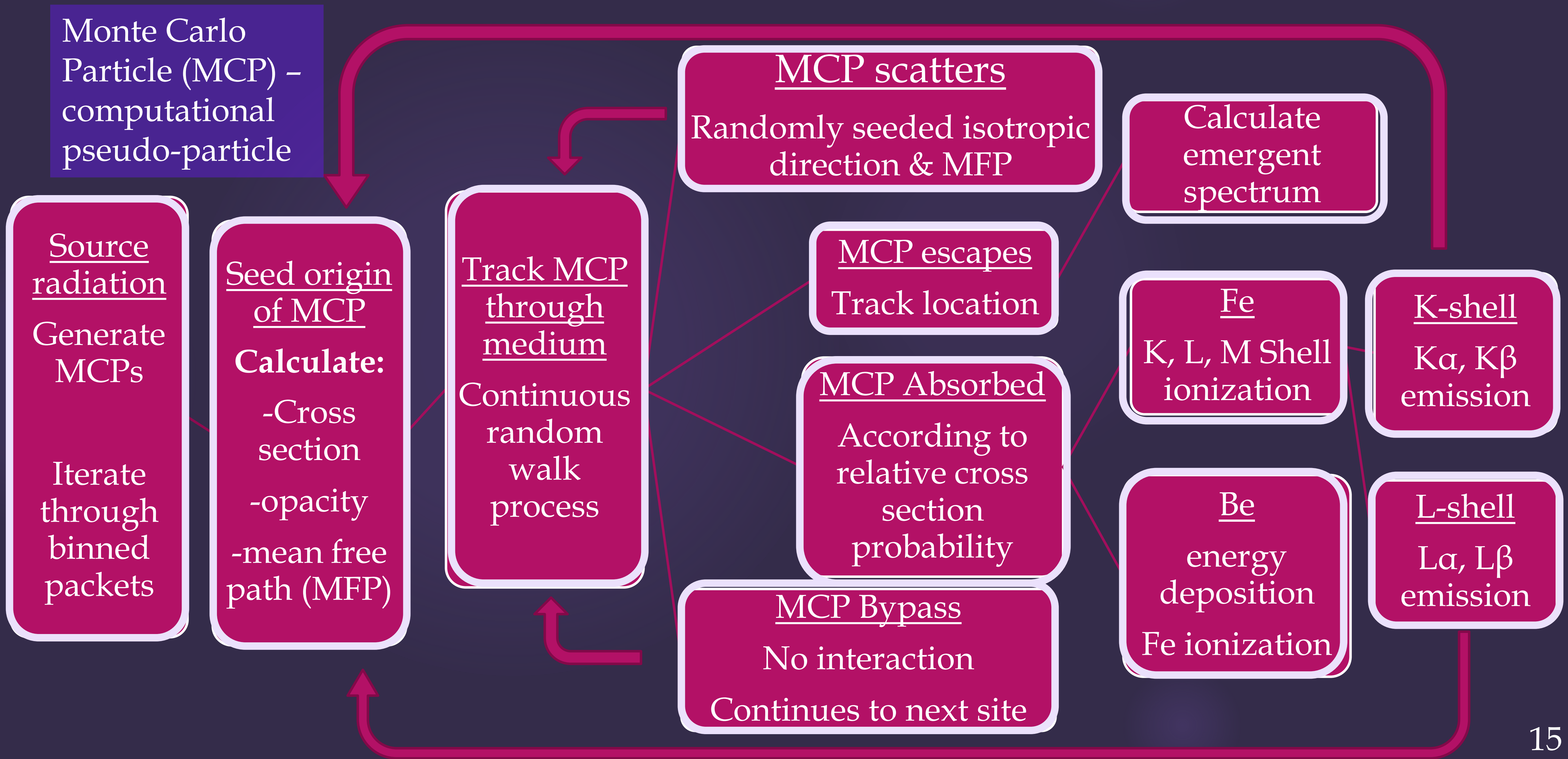

Radiation transport kinetics defined by core radiation field and screened-hydrogenic atomic data package

Radiation Field

- Defined by emissivity of thermal core radiator:

$$j_{f\rightarrow f}\left[\frac{W}{eV\cdot cm^3}\right] = \frac{2\times 10^{-32} n_{ion} n_e Z^2}{\sqrt{T_e}} e^{\frac{hv}{T_e}}$$

  - Input variables:
  - $n_e = n_{ion} = 10^{23}$ cm^{-3}
  - Z ~ 1 (core nearly pure hydrogen)
  - T_e, *hv*, Δ*hv*, radius, height

- Radiation field discretized:
  - binned energies (Δ*hv*), emissivity, and # photons
  - "Monte Carlo Particle (MCP)"

Computational Atomic Data Package

Employs screened-hydrogenic, super-config treatment of atomic structure to calculate:

- Statistical Weights
- Energy levels
- Binding Energies
- Transition Energies
- Screening Factors
- Oscillator Strengths
- Radiative Decay Rates
- Individual Autoionization Rates
- Total Autoionization Rates
- Fluorescence Yield
- Photoionization cross section
- Gaunt-corrected photoionization cross sections
- Collisional Ionization
- Collisional excitation

Monte Carlo Application:

- Seeding particle origins
- Randomized mean free path (in units of energy-dependent attenuation length)
- Selection of interaction event (cross section probabilities)
- Isotropic Scattering

Code tracks MCP trajectory and interaction events

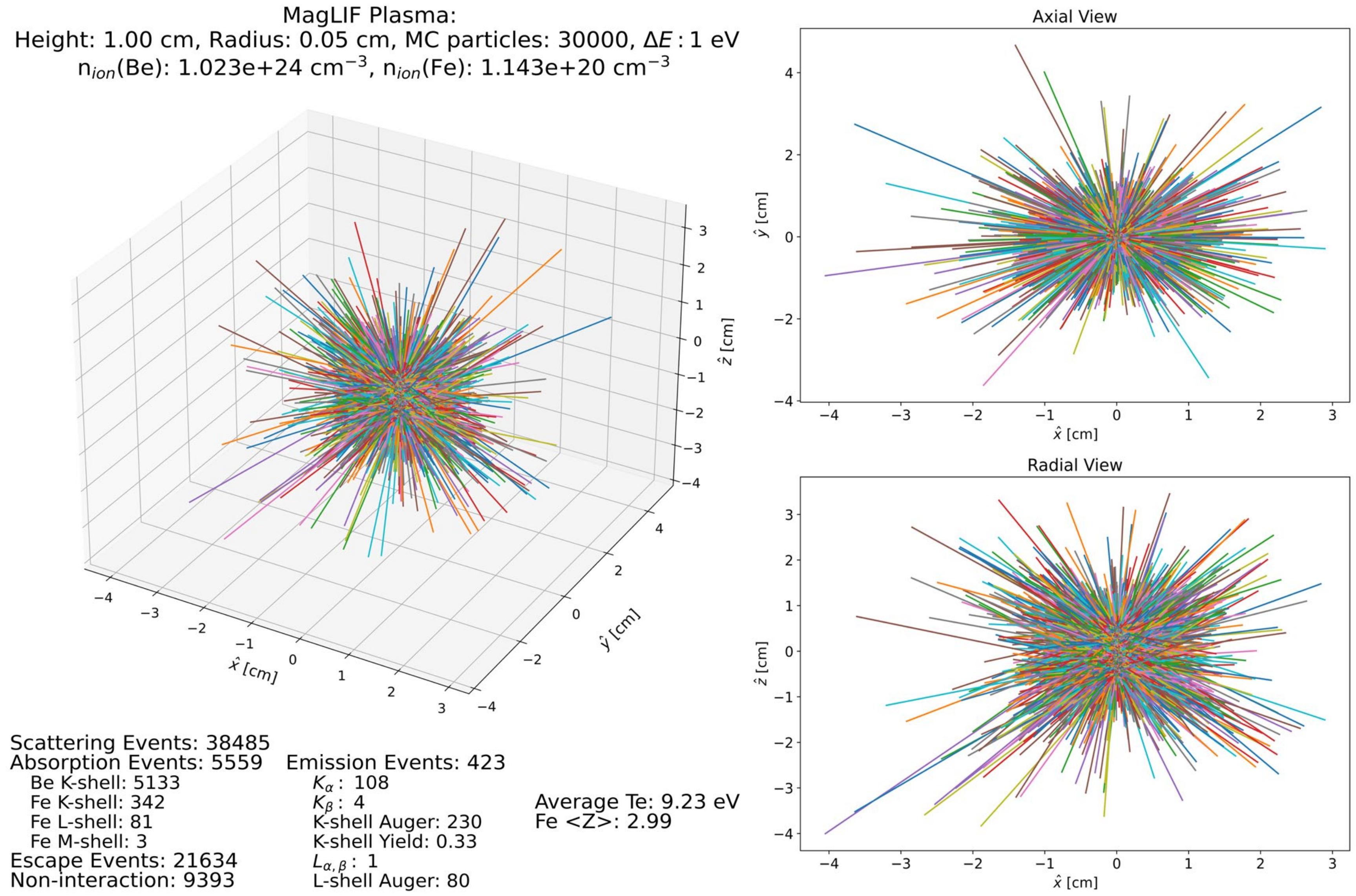

Radiation Field

- Cylindrical core
- 100 µm radius
- 1 cm height
- 2.7 keV thermal temperature
- 100 eV – 31,000 eV range w/ 1 eV resolution

Plasma Medium

- 500 µm shell radius
- 15 g/cc Be (~1.03 x 10^{24} ion/cc)
- 114 ppm Fe (1.1426 x 10^{20} ion/cc)
- Baseline ionization:
  - Fe <Z> ~ 3-5
  - Be <Z> ~ 2

Calculated T_e shows good agreement with MagLIF liner T_e: ~10 eV[1,2]

[1]S. B. Hansen et al., Phys. Plasmas, 25, 056301 (2018) [2]R.R. Childers et al., Contributed Talk, Division of Plasma Physics, Oct. 17, 2022, Spokane, WA

Code tracks MCP trajectory and interaction events

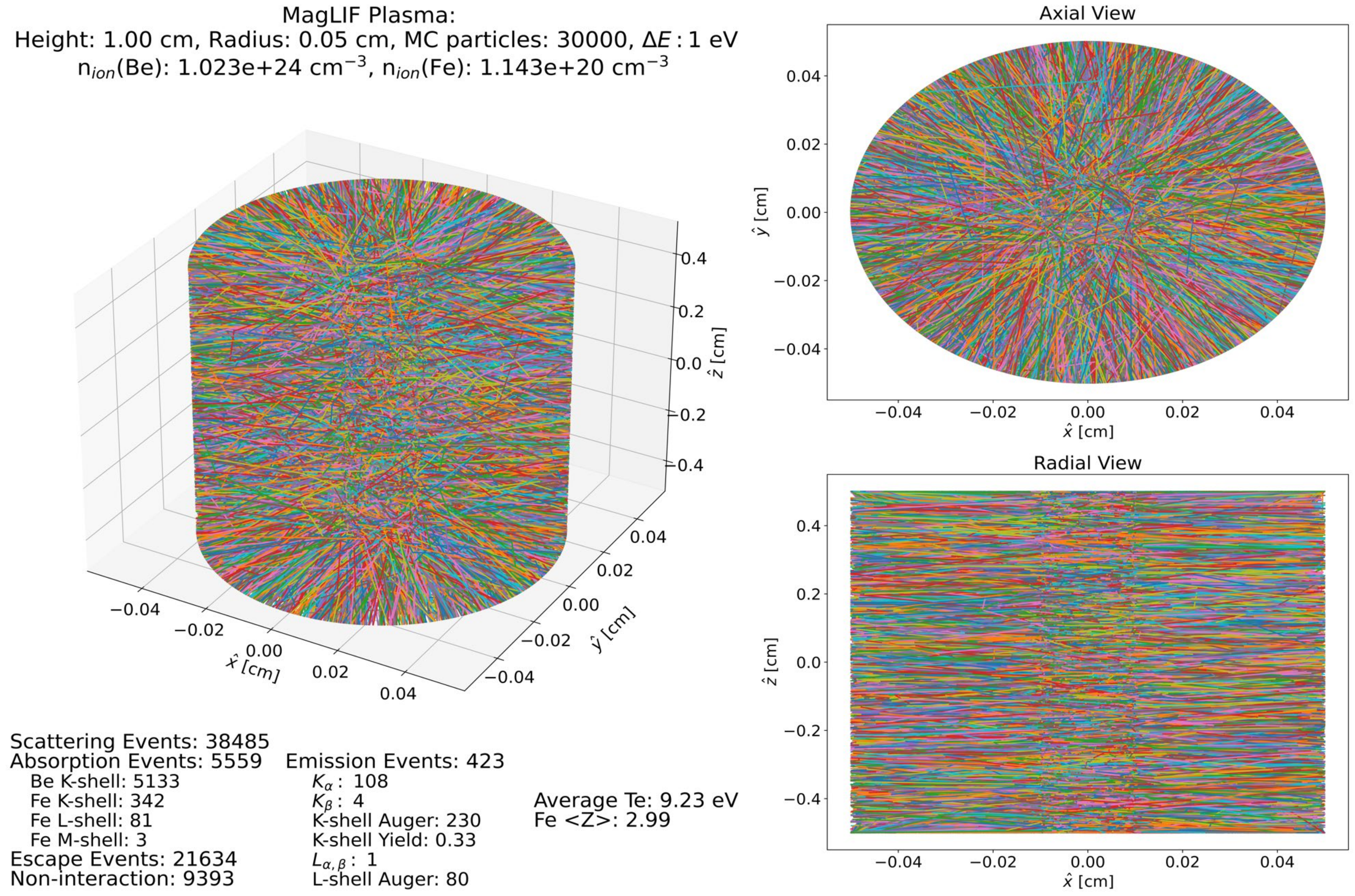

Calculated T_e shows good agreement with MagLIF liner T_e: ~10 eV[1,2]

Radiation Field

- Cylindrical core
- 100 μm radius
- 1 cm height
- 2.7 keV thermal temperature
- 100 eV – 31,000 eV range w/ 1 eV resolution

Plasma Medium

- 500 μm shell radius
- 15 g/cc Be (~1.03 x 10^{24} ion/cc)
- 114 ppm Fe (1.1426 x 10^{20} ion/cc)
- Baseline ionization:
  - Fe <Z> ~ 3-5
  - Be <Z> ~ 2

[1]S. B. Hansen et al., Phys. Plasmas, 25, 056301 (2018) [2]R.R. Childers et al., Contributed Talk, Division of Plasma Physics, Oct. 17, 2022, Spokane, WA

Code independently tracks nonthermal K-shell emission

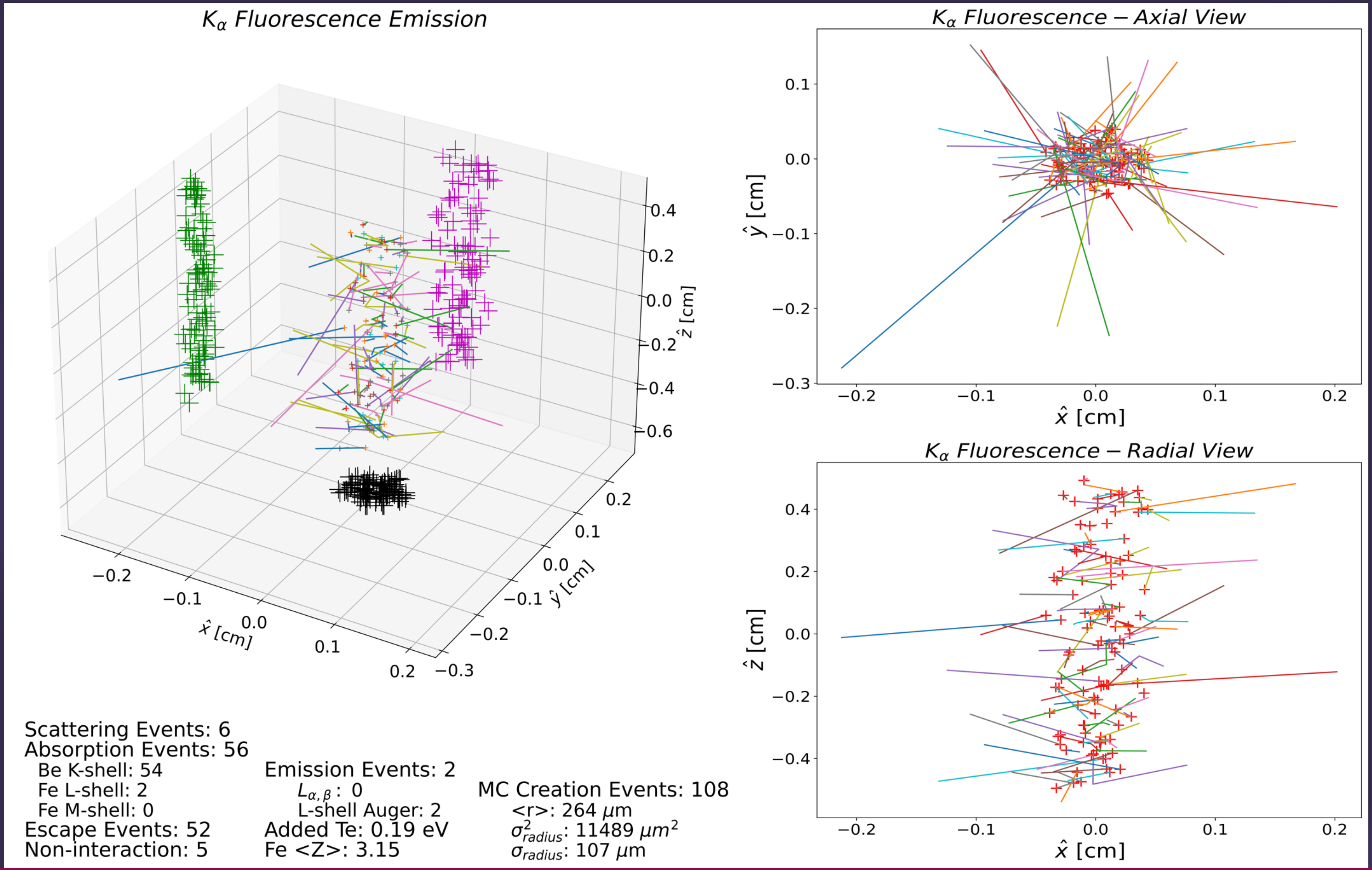

- Spatial statistics performed on K-shell photon origin
- Calculations suggest a region of production averaging 264 μm from pinch axis with a broad spatial distribution (σ ~ 107 μm)

Code independently tracks nonthermal K-shell emission

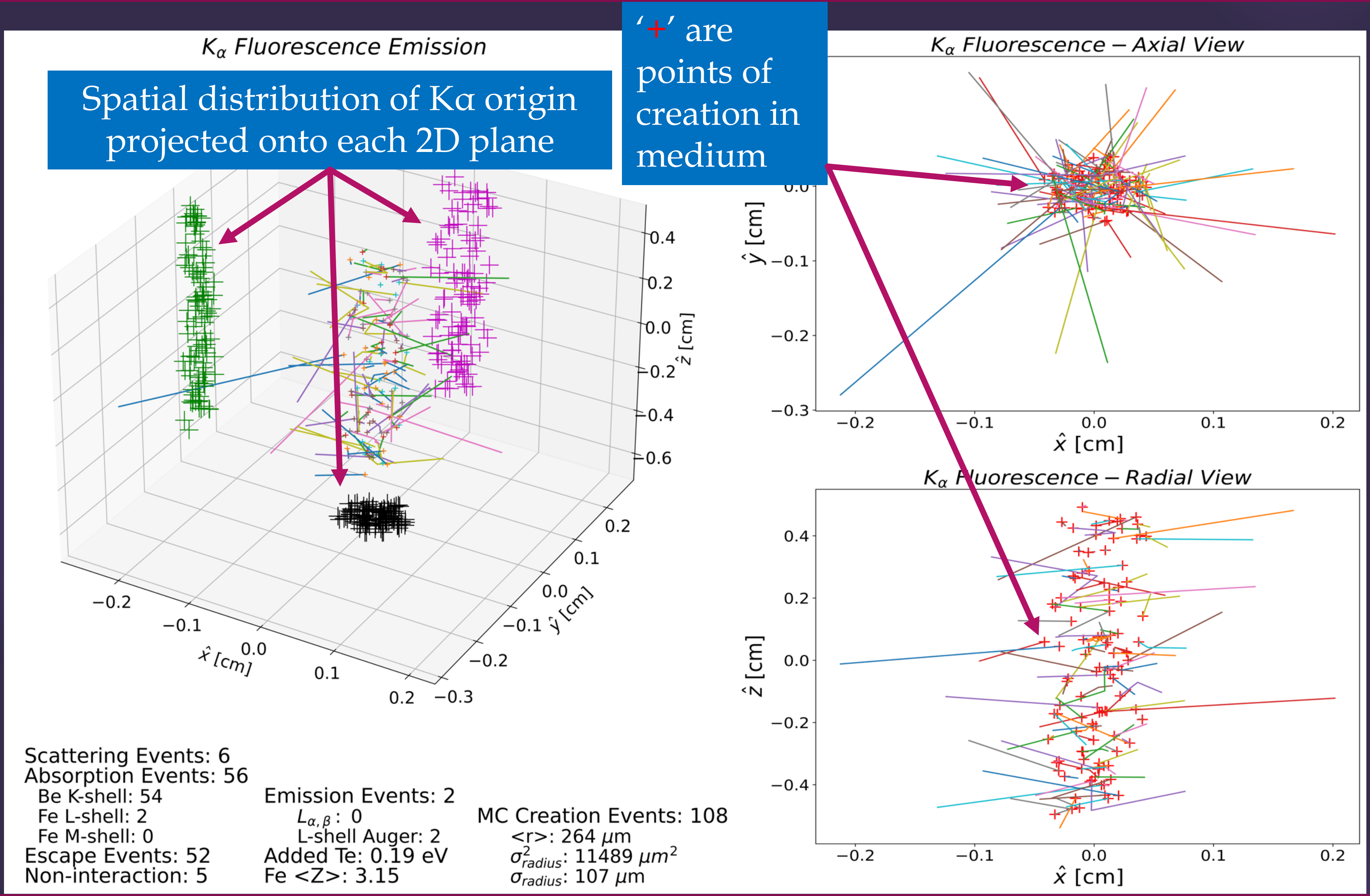

- Spatial statistics performed on K-shell photon origin
- Calculations suggest a region of production averaging 264 μm from pinch axis with a broad spatial distribution (σ ~ 107 μm)

Code calculates emergent transmission spectrum with escaped Fe fluorescence

Line Energies:

1) SH atomic data package (less accurate)
2) Linked database to FAC calculated transition energies, config-averaged

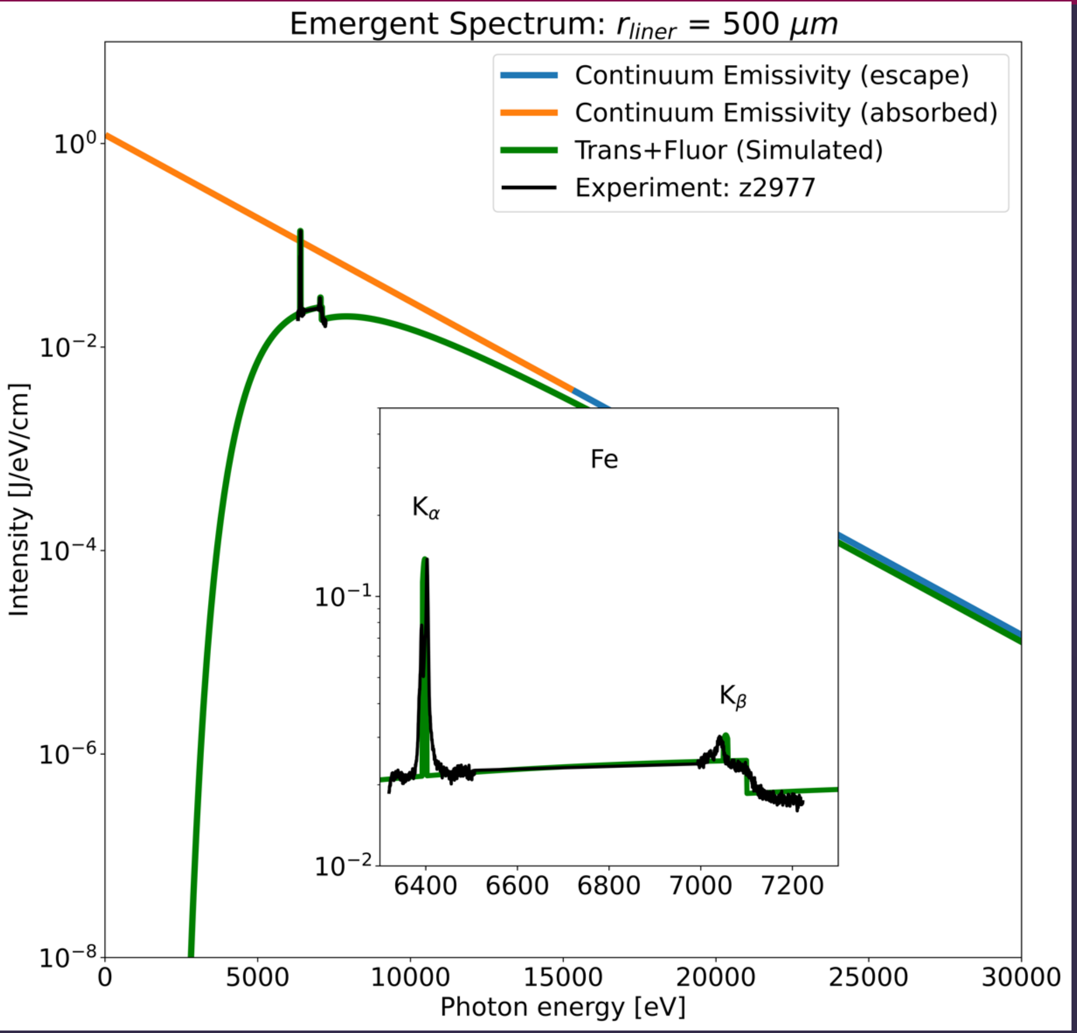

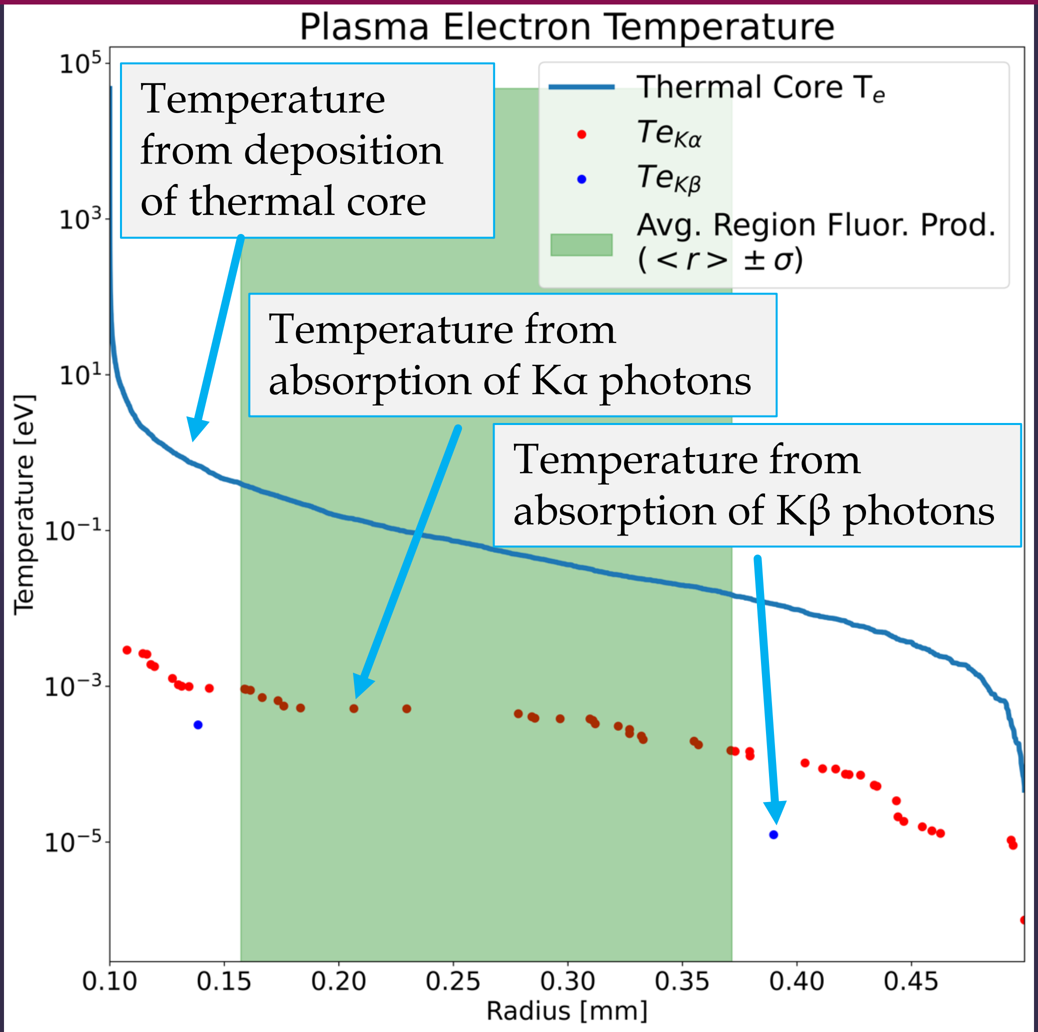

Fe Kα/Kβ show good agreement with Z XRSSS data (provided courtesy of Drs. Eric Harding via Stephanie Hansen)

Radial temp. profile = strong energy deposition nearest thermal core → Plasma temp. gradients

Code calculates emergent transmission spectrum with escaped Fe fluorescence

Line Energies:

1) SH atomic data package (less accurate)

2) Linked database to FAC calculated transition energies, config-averaged

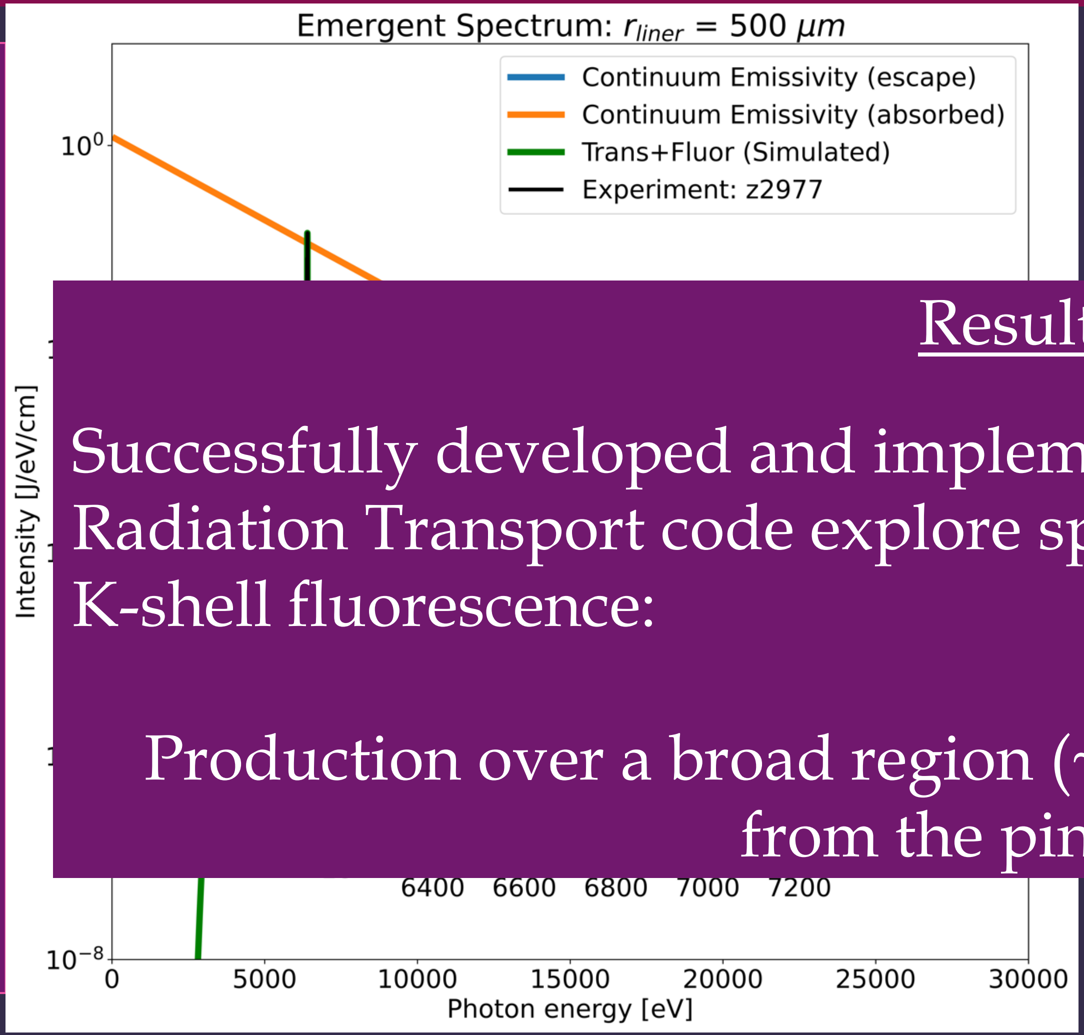

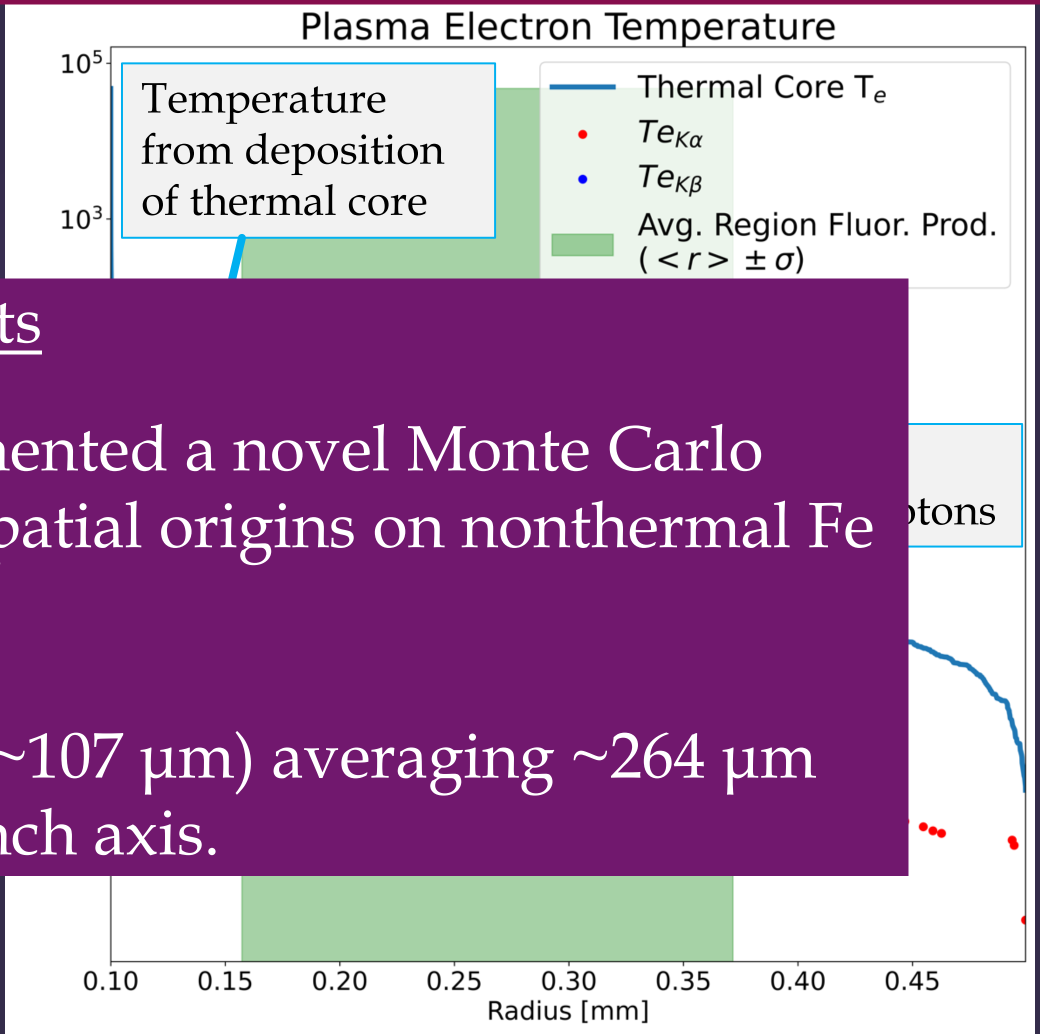

Results

Successfully developed and implemented a novel Monte Carlo Radiation Transport code explore spatial origins on nonthermal Fe K-shell fluorescence:

Production over a broad region (~107 μm) averaging ~264 μm from the pinch axis.

Fe Kα/Kβ show good agreement with Z XRSSS data (provided courtesy of Drs. Eric Harding via Stephanie Hansen)

Radial temp. profile = strong energy deposition nearest thermal core → Plasma temp. gradients

Conclusions

Thank you to the Krell Institute and the LRGF for providing me with an inimitable opportunity.

Thank you to Kris, Shelly, and Michelle for all your patience and support through my years in the program.

<u>The research presented was made possible thanks to a collection of collaborators:</u>
Drs. David Ampleford and Stephanie Hansen of Sandia National Laboratories
The experimental team performing experiments on Zebra at UNR, including Dr. Victor Kantsyrev, Dr. Ishor Shrestha, and Veronica Shlyaptseva.
This work was supported by NNSA through the Krell Institute Laboratory Residency Graduate Fellowship under DE-NA0003960 and by NNSA under DE-NA0003877 & DE-NA0004133.